IMPROVEMENTS OF WARM-SEASON CONVECTIVE WIND FORECASTS AT THE KENNEDY SPACE CENTER AND CAPE CANAVERAL AIR FORCE STATION

by

ANDREW N. LOCONTO

B.S., Plymouth State University, 2005

THESIS

Submitted to Plymouth State University

in Partial Fulfillment of

the Requirements for the Degree of

Master of Science

in

Applied Meteorology

December, 2006

This thesis has been examined and approved.

Thesis Director, James P. Koermer
Professor of Meteorology
Department of Chemical, Earth, Atmospheric, and
Physical Sciences

Joseph Zabransky, Jr.
Professor of Meteorology
Department of Chemical, Earth, Atmospheric, and
Physical Sciences

Thomas R. Boucher
Assistant Professor of Statistics
Department of Mathematics

Date

ACKNOWLEDGEMENTS

I am indebted to many people; to name them all here in this space would indeed be difficult. I would first like to extend sincere thanks to the New Hampshire NASA Space Grant Consortium for the funding of my research at the Kennedy Space Center in the summer of 2005 and to NOAA/NWS for supporting my graduate studies. I also offer my sincere thanks to Dr. James Koermer of the Judd Gregg Meteorology Institute at Plymouth State University, for selecting me to join him in the initial research in the summer of 2005, for the design of the programming scripts we used that summer, and for the many suggestions and guidance he provided to me in this thesis.

I would also like to thank the members of the 45th Weather Squadron and the Applied Meteorology Unit at Kennedy Space Center for the wind tower data and their guidance and suggestions toward this project.

I also would like to thank my thesis committee members, Dr. Koermer, Dr. Joseph Zabransky Jr., and Dr. Thomas Boucher, for reviewing my thesis and providing me with additional suggestions to make this thesis stronger.

In addition to my thesis committee members, I would like to thank the rest of the PSU Meteorology Department faculty (Drs. Lourdes Avilés, Eric Hoffman, Samuel T.K. Miller and Mr. Brendon Hoch) for their guidance and for my undergraduate and graduate education, which equipped me with the skills to complete this project. A special thank you to Dr. Hoffman and Dr. Miller for allowing me to complete semester research projects directly related to this Master's Thesis.

I would like to offer special thanks to Betsy Dupont and Kristin Cummings, who worked diligently over the past summer with Dr. Koermer to look at the 2004-2005 years and allowed me to use their data as a part of the project.

I also would like to thank and extend best wishes in the future to my graduate school classmates and friends—the “first wave” of PSU Meteorology graduate students—Rachel Cloutier, Kimberly Jeffs, and Melissa Wellman. We’ve been through a lot during the last five years, but through support and friendship we can now call ourselves M.S. graduates! I would like to also thank my friends that I have met through various stages of my five-year education here at PSU. Specifically, I’d like to thank Bridget Bixby, Stephen Dialessi, Thomas Feeley, Katie Francoeur, Laura Levesque, Christopher Popieniek, Lindsay Tardif, and Jessica Whitaker.

Lastly, but most importantly, I am forever indebted to my parents, Andrea and Frederick Loconto, who through many years of sacrifice allowed me to get a strong education all the way through graduate school. I can only hope that they are happy with the person I have become and the career that I have chosen. They watched my growth from a young boy sitting on the front porch amazed at the sight of lightning flashing across the sky to the meteorologist that I have now become. I am forever grateful, Mom and Dad, and I love you both very much.

TABLE OF CONTENTS

LIST OF TABLES

LIST OF FIGURES

ABSTRACT

IMPROVEMENTS OF WARM-SEASON CONVECTIVE WIND FORECASTS AT THE KENNEDY SPACE CENTER AND CAPE CANAVERAL AIR FORCE STATION

by

Andrew N. Loconto

Plymouth State University, December, 2006

The purpose of this thesis was to evaluate current convective wind gust forecasting tools and develop both an extensive climatology of warm-season convective wind gusts and some new convective wind gust forecasting techniques for potential operational use at NASA's Kennedy Space Center and Cape Canaveral Air Force Station (KSC/CCAFS). The primary dataset used was an 11-year (1995-2005), May through September series of 5-minute averaged peak wind speeds from an extensive instrumentation network of towers on the KSC/CCAFS complex. After rigorous manual and automated quality control routines were performed on the dataset, a chronological dataset of "convective wind periods"—periods in which a peak wind gust was recorded when a thunderstorm(s) was occurring over a length of not more than 6 hours—was compiled. Climatological statistics were then computed for the 11-year warm-season convective wind periods.

After dividing up these convective wind periods into "KSC warning-criteria"—convective wind periods where peak wind speeds were ≥ 35 knots and

"below-criteria" periods, an evaluation of current forecasting aids using RAOB and Doppler radar data for a pool of convective wind periods was performed. The RAOB data used in this study came from the most recent local KXMR sounding for any convective wind period, while the Doppler radar data utilized in this study was from the NCDC's archive of the Melbourne, FL (KMLB) "Storm Structure" datafile from 5 minutes prior to the occurrence of the maximum peak wind gust for any convective wind period. This study found Probability of Detection (POD) and False Alarm Rate (FAR) values of roughly 50% for the commonly-used binary (yes/no) RAOB-based convective wind forecast aids, MDPI and WMSI, for differentiating between warning-criteria and below-criteria peak wind gusts. Root-mean-squared (RMS) errors for RAOB-based peak wind gust forecasting tools (WINDEX, T1, T2 and Snyder Method) were found to be undesirably high, with RMS errors ranging between 9 to 21 knots. Using the Doppler radar data, much more accurate RMS error values of maximum peak wind speeds were reported using a 44-case dataset by using Echo Top/VIL (ET/VIL) Wind Gust Potential Equation than was reported by a previous study by Sullivan (1999). However, large RMS errors were found for wind speeds below KSC warning criteria. It was also found that cell-based VIL and maximum reflectivity were found to have the best correlation to peak convective wind gust speeds.

Finally, work was done to develop new convective wind forecasting aids using RAOB sounding data and Doppler radar data. It was found that in the mean a potential differentiating factor between KSC warning-criteria gusts and

below-criteria wind gusts was the lapse rate of equivalent potential temperature (theta-e). From this result, threshold values of theta-e lapse rate were established for several central Florida flow regimes as defined in Lericos *et al*. (2000). A multiple linear regression equation was also developed using cell-based VIL, maximum reflectivity and height of the maximum reflectivity as predictors. Using a 22-case independent dataset, slightly better accuracy was found using this new equation than the ET/VIL with much more accurate values reported for below-criteria winds. It was shown that for cell cores whose maximum reflectivities reside above freezing level and that are accompanied by high values of cell-based VIL, a severe convective wind gust (≥ 50 knots) was found to have occurred. The conditions described for severe convective winds from this study (high VIL values accompanied by cell cores above freezing level) would seem to suggest that hail was present just prior to downburst occurrence. This is in general agreement with previous modeling studies of wet microbursts in stable lapse rate regimes.

CHAPTER 1

1. Introduction and background

Convective winds and the associated low-level wind shears these events produce are well-known hazards to aviation and space launch activities. At the Kennedy Space Center (KSC) and the Cape Canaveral Air Force Station (CCAFS), accurate and timely prediction of gusty winds from deep, moist convection is critically important. To that end, the forecasters at the 45th Weather Squadron (45 WS) at KSC/CCAFS issue convective wind advisories for the entire KSC/CCAFS complex for thunderstorms that produce convective winds ≥ 35 knots. A more detailed summary of convective wind warning criteria for KSC/CCAFS, among other warning authorities, is shown in Table 1.

Many research efforts have focused on understanding the processes that generate microbursts. Fujita (1981) defined a microburst as a strong downdraft of air that induces damaging outflow winds with a horizontal extent ranging between 0.4 km and 4 km. Wilson *et al.* (1984) redefined a microburst for use in radar meteorology as the presence of a near-surface radial divergence signature with a velocity difference across the divergence core meeting or exceeding 10 ms^{-1} across a horizontal distance of no more than 4 km. Wakimoto (1985) modified the definition of Fujita (1981) and defined a “wet microburst” as one observed in humid environments that are associated with intense convective precipitation, and a “dry microburst” as one observed in low relative humidity environments that are associated with little or no precipitation reaching

Table 1. Warning criteria table.
Source: Mr. William Roeder, 45 WS

LOCATION	CRITERIA	DESIRED LEAD-TIME
KSC (surface-300 Ft)	≥ 35 Kt	30 min
	≥ 50 Kt	60 min
	≥ 60 Kt	60 min
CCAFS (surface-200 Ft)	≥ 35 Kt	30 min
	≥ 50 Kt	60 min
Patrick AFB (surface)	> 25 Kt	30 min
	≥ 35 Kt	30 min
	≥ 50 Kt	60 min
	Gust Spread ≥ 20 Kt	Observed
	LLWS < 2,000 Ft	Observed
MELBOURNE (surface)	≥ 50 Kt	60 min

the surface. It is the wet microburst that is most commonly observed across the KSC complex in the warm season, owing to the presence of the warm, humid airmass that is characteristic of Florida warm seasons.

Several theoretical and modeling studies have attempted to conceptualize the physics that drives wet microbursts. These studies suggest that evaporative cooling of liquid water and precipitation drag are two physical mechanisms that drive microbursts to the surface (Srivastava 1985, 1987; Proctor 1989). There also appears to be a microphysical dependence on wet microburst strength. A few of these research efforts have concluded that meltwater from hailstones evaporating into a sufficiently dry enough layer promotes significant evaporative cooling for wet microbursts (Srivastava 1987; Proctor 1989). These microphysical findings are supported by observational evidence in Atlas *et al.*

(2004) for an Amazonian wet microburst. In addition, modeling studies by Proctor (1989) found that the presence of a stable layer near ground level would weaken the strength of the wind gusts from microbursts. Using proximity radiosonde soundings from the 1986 Microburst and Severe Thunderstorm (MIST) project, Atkins and Wakimoto (1991) have demonstrated that a change in equivalent potential temperature (θ_e) between the surface and middle-levels of the atmosphere exceeding 20 K was found to be present on wet-microburst days, compared to the same vertical θ_e difference of 13 K or less on null days.

Following Atkins and Wakimoto (1991), Wheeler (1996) developed the Microburst Day Potential Index (MDPI) for operational microburst forecasting at the Kennedy Space Center. This index, to be defined mathematically later, is based upon difference between the maximum θ_e in the low-levels of the atmosphere and the minimum θ_e in the mid-levels of the atmosphere. Following Proctor (1989), McCann (1994) developed the Wind Index (WINDEX), also to be defined mathematically later. WINDEX is an empirical formula that computes a maximum wind gust for a microburst that originates at the melting level. Geerts (2001) modified the WINDEX equation using RAOB soundings for Australian microbursts and defined GUSTEX, an empirical relationship that includes the 500 hPa wind speed in addition to the gust speed calculated by WINDEX.

Both the MDPI and WINDEX may be updated using current surface and RAOB observations, and have also recently been overlaid onto visible or infrared satellite imagery (Ellrod *et al.* 2000; Pryor and Ellrod 2003) as computed from Geostationary Operational Environmental Satellite (GOES) Sounder-derived

soundings. Ellrod *et al.* (2000) found that the GOES WINDEX does a poor job at estimating the wind speed at night due to the more stable surface to melting-level lapse rate at night. More recently, Pryor and Ellrod (2004) developed the Wet Microburst Severity Index (WMSI), which computes the product of Convective Available Potential Energy (CAPE) and the difference in θ_e from the surface to the mid-levels divided by 1000. Like the MDPI and WINDEX before it, WMSI has been overlaid onto visible or IR imagery.

The Air Force (Miller 1975) have developed a number of indices for predicting convective winds. Among them are the T1, T2, and Snyder methods for anticipating convective gusts. However these older indices were primarily based on convection in the Midwestern U.S. and have not been really evaluated for use in areas such as the Florida Space Coast.

WSR-88D Doppler radar can serve as a nowcasting tool for detecting the onset of convectively-generated wind episodes. Roberts and Wilson (1989) have found that descending reflectivity cores, V-shaped reflectivity notches, storm rotation or large values of radial wind convergence within the mid-levels of the storm are characteristic radar signatures of microbursts. These features were observed 2-6 minutes prior to microburst occurrence. This evidence is supported by preliminary research conducted by Falk *et al.* (1998), which defined thresholds for convective wind warnings at the NWS in Shreveport, LA in terms of magnitude and height of reflectivity cores and also in terms of storm-relative radial convergence for single-cell pulse-type thunderstorms. Sullivan (1999) evaluated three wind gust prediction equations that use Doppler-radar measured

variables using KSC mesonetwork data from 15 microburst cases. Of these, he found that the Storm Top/Vertically Integrated Liquid (ST/VIL) equation best predicted KSC microburst events to within +/- 5 knots.

These operational tools have been met with varying degrees of success for convective wind forecasts at the Kennedy Space Center and Cape Canaveral Air Force Station. There is a need to evaluate existing tools and to develop additional forecast indicators of convective wind outbreaks. This need is further stressed by the various space launch functions that Kennedy Space Center performs for the U.S. Space Program, which necessarily mandate accurate and timely prediction of these events.

The purpose of this Master's Thesis is to objectively evaluate most of the current techniques to predict strong convective winds and to design/evaluate additional warm-season convective wind forecasting tools for use at the KSC/CCAFS complex. An updated eleven-year convective wind climatology for the KSC/CCAFS complex will first be presented in order to identify individual convective events, how frequently these events occur and what favors their generation, especially from a thermodynamic perspective. Existing predictive tools for convective winds will then be evaluated for a variety of identified convective events, using both rawinsonde-based techniques as well as Doppler radar techniques. Then new or modified forecasting aids will be examined to predict both the likelihood of these convective wind episodes as well as the maximum expected wind gust with the goal of improving forecast skill of convective wind forecasting at KSC/CCAFS.

CHAPTER 2

2. Data and methodology

a. Climatology

This section will highlight the data and methodology used in the construction of the eleven-year warm-season convective wind climatology at KSC / CCAFS. Much of the following discussion is documented in Koermer and Loconto (2005) for the 1995-2003 convective wind years and Cummings *et al.* (2007) for the 2004-2005 convective wind years. Sections 1 through 4 below are taken from Koermer and Loconto (2005). This updated climatology will serve as a dataset that will be used for the development of rawinsonde and WSR-88D forecasting tools. For this reason, it is worthwhile to discuss how the convective wind climatology was designed as a background before discussing the forecasting tools.

1) CLIMATOLOGICAL DATA

The primary wind data used for the climatological update were the 5-minute peak wind data from sensors on 44 towers on or around the CCAFS/KSC complex for the months of May through September for 1995 through 2003. The NASA Applied Meteorological Unit (AMU) had already completed some automated and manual quality control (QC) on these data. Case and Bauman (2004) give a very complete description of the tower mesonet. They also discuss the automated data QC methodologies that they adopted from Lambert (2002)

and their additional manual QC of tower temperature data to build what is referred to as the “AMU QC data”. This dataset was the starting point for the development of our updated climatology.

2) INITIAL DATA PROCESSING

The AMU QC data were provided in individual monthly files for each tower sensor suite. Since most of the sites had sensors at more than one elevation and several towers have dual sensors on opposite sides of the tower, there were a total of 151 data files per month containing the 9 years worth of data for the individual sensor suite. Files were identified by tower number, month, and sensor elevation. Dual sensors on different sides of a tower are usually given different tower identifier numbers. Figure 1 depicts the location of various towers on or around the CCAFS/KSC area.

Wind tower data were in plain ASCII tabular, semi-colon delimited format and each line contained possible entries for identification number, year, month, day, hour, minute, elevation, temperature, dewpoint, wind speed, wind direction, peak wind speed, peak wind direction, directional variability, and relative humidity. Missing data or data replaced in the AMU QC process had numerical entries like -999x, where x was 9 for missing data and other numerical digits when substituted after various QC processes.

In order to get a better idea on the frequency of occurrence of high wind events (≥ 35 knots) that would have required 45 WS warnings, tower data were read in and a single file was built for each month and year containing the observations from all locations where the peak wind exceeded 24 knots. Files

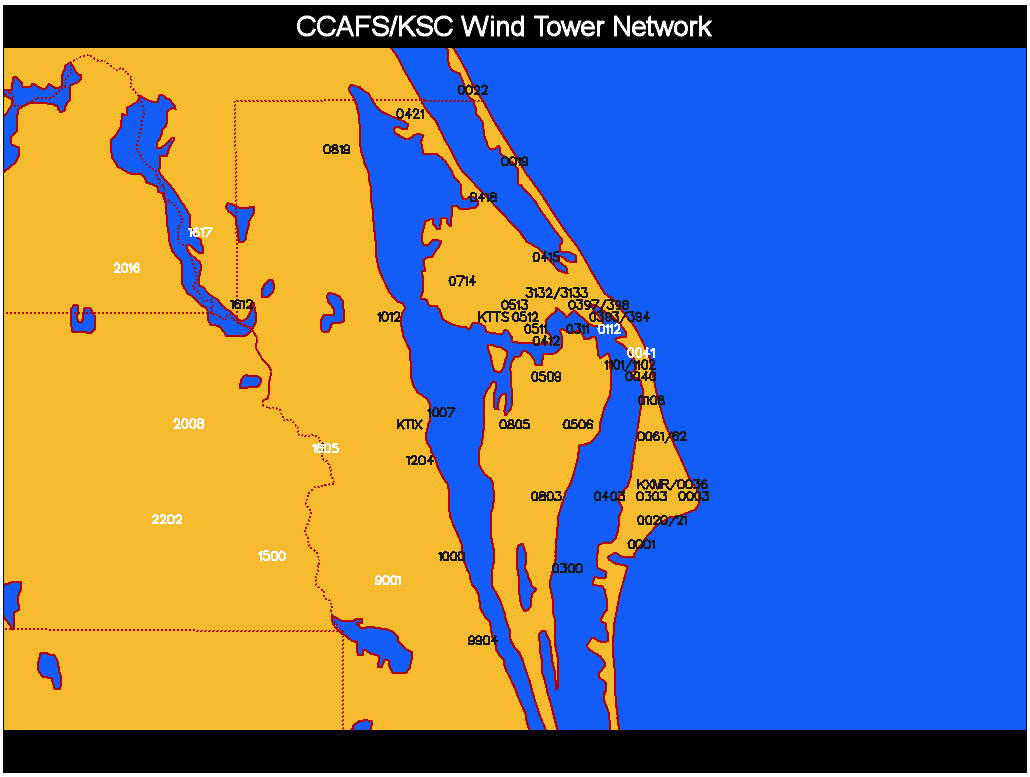

Figure 1. CCAFS/KSC tower network. White shading indicates tower ID numbers that were excluded in the study.

were then imported into an EXCEL spreadsheet and observations were then sorted in chronological order. This allowed us to see “outbreaks” and not just single events. After reviewing the data in these files, a problem was discovered at several sites. The problem was that some locations had continuously steady 5-minute values of peak wind for hours or (in one case) for even days. Besides a constant peak wind value, the directional variability was listed as 0 or 1 degree—highly suspect for even weak winds. There was also no corresponding meteorological support to justify these extended events. To remedy this, a program was developed to look for any wind variability entries of 0 or 1 degrees with peak winds at or above 5 knots and replace the peak wind gust, peak wind direction and directional variability values with a “-9997” flag. The program was

then run on the initial quality controlled data and the corresponding chronological EXCEL files were rebuilt.

3) INITIAL MANUAL ASSESSMENT

Using each monthly file as a guide, a manual evaluation was used to try to assess if a strong wind report or a series of strong wind reports could be associated with convection or some other alternative feature like a strong pressure gradient (PG) from a tropical system or a plain synoptic gradient. The EXCEL spreadsheets were color-coded accordingly and used green cell shading or probable convective events, no shading for probable strong PG driven events, and red shading for observations that defied any meteorological explanation. In performing these assessments, we used radar, satellite imagery, lightning data, surface observations and reanalysis data, and surface observations from the NASA Shuttle Landing Facility (ICAO: KTTS).

Radar data included NCDC archived NEXRAD radar maps and archived Plymouth State University (PSU) archived MDR and RCM maps. The NCDC maps were quite limited during 1995 through early 1996, but were the only radar data readily available. NCDC radar maps were available at the following site:

http://www4.ncdc.noaa.gov/cgi-win/wwcgi.dll?wwNexrad~Images2

for only about one hour (usually ~23 Z) per day from 1995 through early 1997 and then generally became available on an hourly basis. However, the resolution of the US composite maps was quite poor when looking to distinguish the location and intensity of convective mesoscale features

The PSU radar data could be custom mapped for the region of interest and were retrieved from http://vortex.plymouth.edu/u-make.html. The PSU hourly MDR data were available for 1999 and beyond and provided a bit more detail about intensity, but spatial resolution is very broad-brushed. The PSU twice-hourly RCM data became available for 1992-1993 and provided very good 10-km echo resolution radar imagery. Figures 2a-c, all for the same approximate date/time, show the limitations or benefits with using these various forms of radar data.

For cases where radar data for a particular date/time were missing, hourly infrared satellite images from the PSU archived web site listed above were accessed. Satellite data are archived as broad view images and hence have resolution limitations, similar to some of the radar maps. Figure 3 provides example of this imagery for the same date/time as used in Figure 1. This example does clearly show the convective cloud tops in the area of interest. For lightning data, we used the AMU Cloud-to-Ground Lightning Surveillance System (CGLSS) Climatology as another tool to identify convective and non-convective events. This CGLSS climatology provided a daily summary of strikes and hence did not provide good time resolution.

The 00 and/or 12 UTC regional height-contoured 1000mb NCEP/NCAR reanalysis maps or hourly pressure-contoured surface maps, and both were from the PSU archive site to subjectively determine pressure gradient existence and relative strength. The NCEP/NCAR data were used for 1995 through July of 1997 and then the hourly observational data was used from August 1998 through the

end of the study period. The higher time and spatial resolution of the different data sets was sometimes significant. Figure 4 shows the difference in trying to assess the PG strength for 17 UTC on May 31, 2002. The 12 UTC data shows a stronger PG situation than the actual 17 UTC surface data that was taken very close to the time of convection.

The KTTS surface observations for 1995-1998 were obtained from the Air Force Combat Climatology Center (AFCCC) and for 1999-2003 from the PSU archived data site. These detailed observations, taken by very skilled observers, tended to fully corroborate convective assessments from other sources and perhaps provided the greatest details for determining the onset and termination of convection in the area of interest.

After reviewing the various kinds of data, we annotated our strong wind cases with comments on the strength and amount of convection (primarily from radar reports), the strength and direction (if any) of the PG situation, and relevant convective data and gusts (if any) from the KTTS observations. Table 2 shows a spreadsheet excerpt showing two events, where the first has winds attributed primarily to the pressure gradient and the last due to convection. Table 3 shows similar entries for a case identified as “bad” that were missed by QC programs.

4) AUTOMATED PROCESSING OF DATA

While manual analysis of strong peak wind reports was possible, doing the same for over 5.5 million total peak wind reports was not practical. As a result a more automated approach had to be taken to analyze data as being convective

or not. In order to come up with such a scheme, it was first necessary to come up with a convective event database. To accomplish this, convective report data.

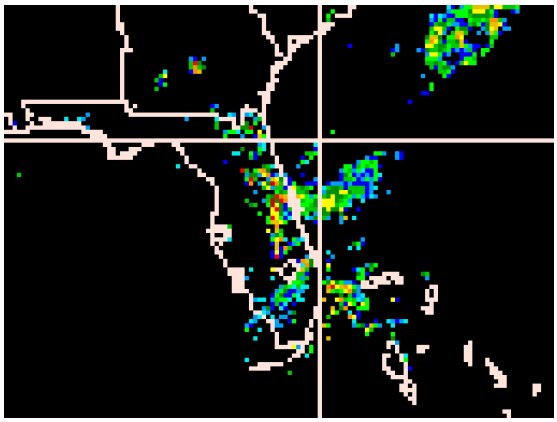

(a)

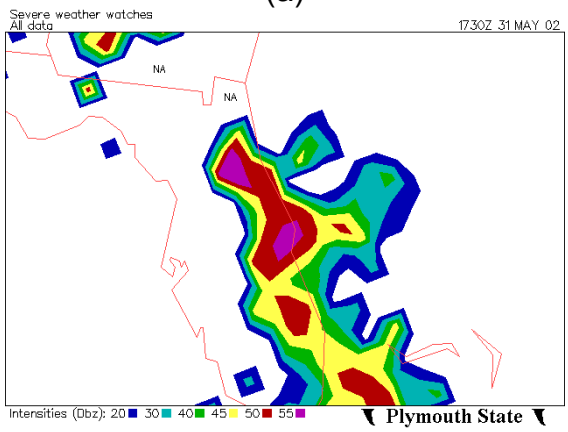

(b)

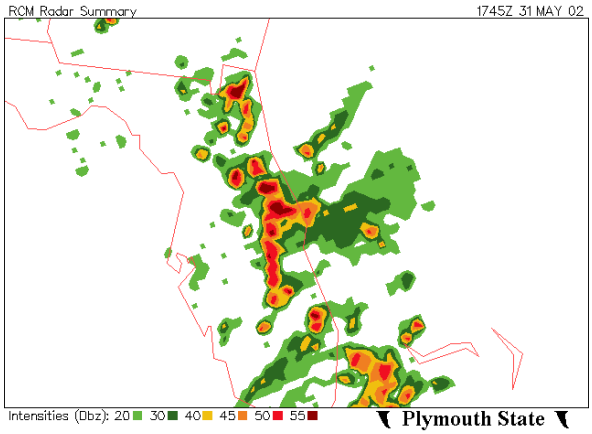

(c)

Figure 2. (a) NCDC NEXRAD , (b) PSU MDR, and (c) PSU RCM radar summary maps for between 1700-1800 UTC on May 31, 2002.

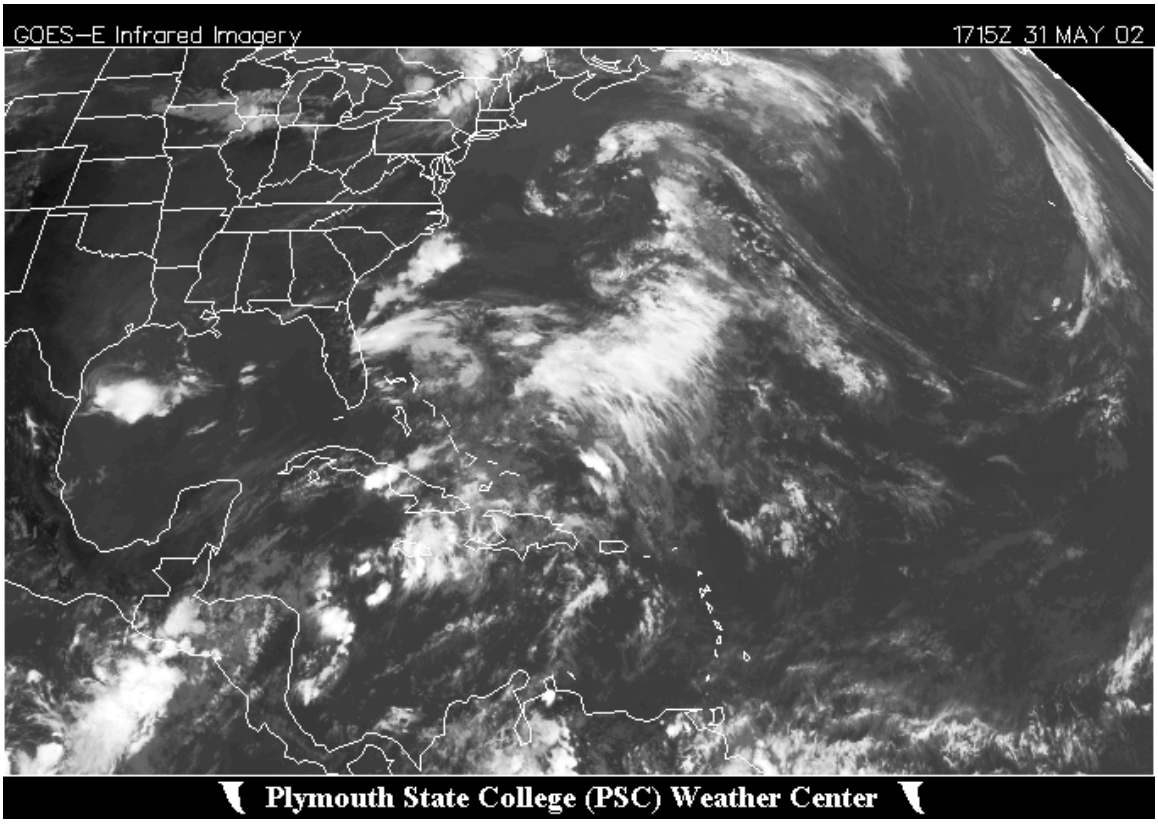

Figure 3. PSU archived infrared satellite imagery for 1715 UTC on May 31, 2002.

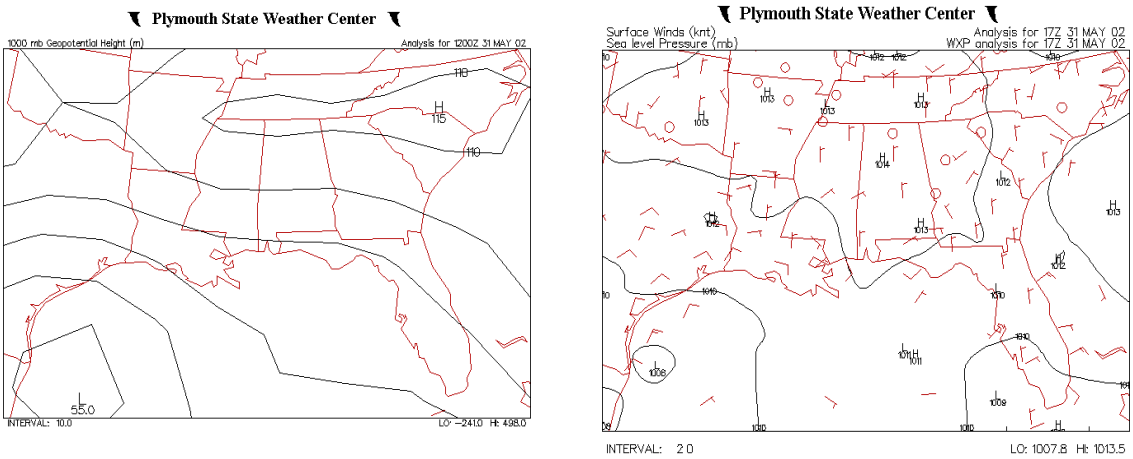

(a) (b)

Figures 4. (a) PSU NCEP/NCAR 1000 hPa height analysis fo1112 UTC on May 31, 2002 and (b) PSU surface analysis for 17 UTC on May 31, 2002.

Table 2. Excerpt from spreadsheet containing peak wind speed (PWS) wind reports ≥ 35 knots for May 2002. The “Original File” column is highlighted in green for those outbreaks attributed to convection and not highlighted for PG-driven events.

. Original File	Year	Mo	Day	Hr	Min	Temp	TD	WS	WD	PWS	PWD	DV	RH	Remarks
3132_05_492.	2002	5	22	15	50	70.9	59.5	29	7	36	5	7	67	No conv, strng NE PG, mdt CU, RW- & G28
0398_05_060.	2002	5	22	16	0	73.4	62.1	20	1	35	360	7	68	" " "
0393_05_060.	2002	5	22	16	20	73.8	63.3	21	5	35	6	9	70	" " "
0393_05_060.	2002	5	22	16	30	73.8	64.2	21	1	36	1	9	72	" " "
0393_05_060.	2002	5	22	16	35	73.8	63.9	23	2	37	359	9	71	" " "
0398_05_060.	2002	5	22	16	35	73.6	63.3	23	358	36	353	7	70	" " "
3132_05_295.	2002	5	22	16	55	-9999	-9999	26	4	35	6	13	-9999	" " "
0003_05_054.	2002	5	22	22	10	66.7	-9999	27	9	35	12	9	-9999	" " "
0398_05_060.	2002	5	23	0	30	73.6	66.4	27	38	35	40	9	78	" " "
3132_05_492.	2002	5	23	0	35	71.4	62.4	28	52	35	51	6	73	" " "
0020_05_090.	2002	5	31	16	55	-9999	-9999	23	125	36	140	21	-9999	Strng conv, vry wk vrbl E PG, TRW & G26
0020_05_145.	2002	5	31	16	55	-9999	-9999	26	130	38	145	21	-9999	" " "
0020_05_204.	2002	5	31	16	55	75.6	-9999	26	132	37	139	21	-9999	" " "
0021_05_090.	2002	5	31	16	55	-9999	-9999	26	126	35	143	22	-9999	" " "
0021_05_145.	2002	5	31	16	55	-9999	-9999	28	128	36	140	22	-9999	" " "
0021_05_204.	2002	5	31	16	55	75.2	69.3	29	132	36	146	22	82	" " "
0003_05_054.	2002	5	31	17	0	74.1	-9999	27	146	36	143	22	-9999	" " "
0020_05_054.	2002	5	31	17	0	74.5	70.7	21	136	35	143	23	88	" " "
0020_05_090.	2002	5	31	17	0	-9999	-9999	25	137	36	143	22	-9999	" " "
0020_05_145.	2002	5	31	17	0	-9999	-9999	27	140	36	141	22	-9999	" " "
0020_05_204.	2002	5	31	17	0	73.2	-9999	28	139	38	140	23	-9999	" " "
0021_05_090.	2002	5	31	17	0	-9999	-9999	26	141	36	138	24	-9999	" " "
0021_05_145.	2002	5	31	17	0	-9999	-9999	28	140	36	140	24	-9999	" " "
0021_05_204.	2002	5	31	17	0	73.2	69.1	29	142	37	143	23	87	" " "

Table 3. Excerpt from June 2002 spreadsheet identifying probable bad reports at towers 511, 512, and 513 on different days. Red is used to highlight bad report entries and peak wind reports ≥ 50 knots.

Original File	Year	Mo	Day	Hr	Min	Temp	TD	WS	WD	PWS	PWD	DV	RH	Remarks
0511_06_030	2002	6	4	13	15	-9999	-9999	53	180	74	180	28	-9999	No conv, vry wk SE PG, no spprt at
0513_06_030	2002	6	4	13	15	-9999	-9999	43	180	74	180	33	-9999	" " "
0511_06_030	2002	6	14	13	35	-9999	-9999	42	184	74	180	23	-9999	No conv, wk W PG, no spprt at KTTS
0512_06_030	2002	6	14	13	35	-9999	-9999	-9995	-9995	74	180	20	-9999	" " "
0513_06_030	2002	6	14	13	35	-9999	-9999	42	183	74	180	23	-9999	" " "

from KTTS surface observations were used to build monthly tables for each year. The tables list each day versus each hour and entries were manually extracted based on whether thunder (T) or showers from CBs or nearby CBs were reported. Peak winds or gusts, if reported from the KTTS METAR, were also noted in this database. We did not count distant CB or distant lightning sightings

by the observer as evidence of convection within the area. We annotated the entry as “0” if there was no convection at or near KTTS and we went back and listed “X” for those times that were under the influence of Tropical systems.

Here is a list of the tropical systems that occurred during the period of this study and the dates that they probably affected wind speeds in the area:

- 1995 – Hurricane Allison (5 Jun), Hurricane Erin (1-3 Aug)., and T.S. Jerry (24-25 Aug)
- 1996 – None, although T.S. Arthur (19 Jun) may have had a slight impact
- 1997 – None
- 1998 – Hurricane Earl (2 Sep)
- 1999 – None
- 2000 – T.S. Gordon (17-18 Sep)
- 2001 – T.S. Gabrielle (14-15 Sep)
- 2002 – T.D./T.S. Eduoard (4 Sep) with a feeder band
- 2003 – None

Based on the table entries a simple decision matrix was created with “1” representing existing or nearby convection for a particular hour and “0” representing either tropical system influence or no convection hours. At this point, the matrix does not distinguish between convection and PG except for the tropical system events.

All data that had undergone automated QC, but was still manually flagged as bad, was manually modified with a “-9990” bad data flag in the respective data files. Files for sites about 300 feet were eliminated from additional automated processing as well as files for sites with fewer than 75% “valid” peak wind reports for the entire period of record. Statistics were then gathered on all valid peak wind events for categories of ≤ 20 knots and for 5 knot range categories above

20 knots. Similar statistics were generated for those hours that were identified at having existing or nearby convection.

5) EXPANSION OF PERIOD OF RECORD TO INCLUDE 2004-2005 AND OTHER MODIFICATIONS

Cummings *et al.* (2007) set out to add to the existing nine-year convective wind climatology developed in Koermer and Loconto (2005) by using the 2004 and 2005 convective wind years. Instead of from the AMU, the raw 5-minute peak wind gust data were acquired from Computer Science Raytheon (CSR). These additional two years of data were first processed using the same manual and automated QC routines outlined above and in Koermer and Loconto (2005). After these manual and automated QC routines were performed, an additional program was created that generated statistics for each convective wind day in the 11-year climatology with output that included the number of observations and time periods that various peak wind speeds (in 5-kt incremented bins) had occurred, as well as the value and time that the maximum peak wind gust had occurred on that day. A breakout such as that described above for each day in the 11 years was found to be extremely useful, as it facilitated the selection of warning-criteria days and below warning criteria days in the development of new convective wind forecasting tools.

6) GENERAL CLIMATOLOGICAL SUMMARIES

After the manual and automated QC was complete, the peak wind data was organized into Microsoft Excel. Yearly, monthly, and hourly statistics of convective wind observations ≥ 35 knots were then created. The same statistics

were then generated for the "convective wind outbreaks." The definition of a "convective wind outbreak" that will be adopted in this thesis is defined by Koermer and Loconto (2005) as the following:

> Convective wind ***outbreaks*** are defined as "peak wind report(s) of ≥ 35 knots, determined to be convectively driven, for a single tower or towers that end with a break in convection of 6 hours or more."

To gain a sense of the frequency of these KSC warning-criteria wind speed occurrences, monthly frequency diagrams of all wind speeds (i.e. convectively-generated and not convectively-generated) < 20 knots and convective wind speeds < 20 knots were generated. Convective wind speeds ≥ 35 knots are then separated into wind speed categories of 5 knot increments. Monthly and hourly distributions of these categorical wind speeds were then developed. To see if there is a height dependency on these convective wind speeds, the categorical convective wind speeds are then sorted by the tower elevation that the wind speed was measured. Because some towers report wind data at the same elevation and not others, the number of convective wind speeds for each wind speed category was normalized by dividing by the number of towers that report at that elevation. This removes any bias that an irregular number of tower measurements would have at each elevation.

7) THERMODYNAMIC CLIMATOLOGY SUMMARIES

Once the eleven-year climatology was created, a listing of all convective wind outbreaks that took place during the eleven-year climatology was constructed. A pool of 33 convective wind episodes was taken from this listing.

A second pool of 33 null events (i.e. those events that produced thunderstorms but not cases in which warning-criteria convective winds were reported by the KSC mesonetwork) was also compiled. The most recent Cape Canaveral radiosonde observation (KXMR) was taken for each of the 66 events. In almost all cases, the most recent XMR radiosonde that was available for analysis was the 15Z radiosonde data. This information came in the form of a textfile acquired from Plymouth State University's KXMR Sounding Generator Archive page (http://vortex.plymouth.edu/uacalplt-xmr-u.html). These radiosonde data were imported into Microsoft Excel spreadsheets.

From these spreadsheets, composite graphs showing the distribution of equivalent potential temperature (θ_e, in Kelvin) as a function of height (in meters) were constructed for the convective wind days and null days. To better identify what the theta-e profile would look like on a typical warning criteria versus below warning criteria wind day, a mean profile of θ_e was developed for warning criteria wind days and below warning criteria days by averaging the θ_e in 500-m layer increments for warning-level events and below-warning criteria events. A two-sample t-test was performed to test the statistical significance of these two profiles.

b. Radiosonde forecasting techniques data and methodology

This section will discuss the data and methodology that was used in developing and/or evaluating forecasting tools for the KSC/CCAFS using KXMR radiosonde data. The radiosonde data that was used in this section is the same as that used in building the thermodynamic climatology (see Section 1(g) for

more detail). As will also be the case for the WSR-88D forecasting tools, the RAOB convective wind forecasting tools have an inherent assumption—that there is a sufficiently large enough forecast confidence that convection is likely. These forecast tools have little or no forecasting significance if that assumption is not met.

1) MDPI AND WMSI DEFINITIONS

The Microburst Day Potential Index (MDPI) (Wheeler and Roeder 1996) is a KSC wet microburst forecasting tool, and is defined by Eq. (1) below:

$$MDPI = \frac{\theta e \max - \theta e \min}{30} \tag{1}$$

where θ_{emax} is the maximum θ_e (in Kelvin) in the 1000-850 hPa layer and θ_{emin} is the minimum θ_e (in Kelvin) in the 660-500 hPa layer. The denominator of 30 is a local tuning factor. A value of MDPI > 1 suggests a threat of a wet microburst if convection is likely to occur. Another wet microburst forecasting tool is the Wet Microburst Severity Index (WMSI) (Pryor 2005), defined by Eq. (2) below:

$$WMSI = \frac{CAPE \cdot \Delta \theta e}{1000} \tag{2}$$

Where CAPE is the Convective Available Potential Energy (in J kg^{-1}) and $\Delta\theta_e$ is the same as previously defined. CAPE is used in the WMSI equation to filter out weaker thunderstorms and assumes that storms that are produced in high-CAPE environments are also proficient enough rain producers to promote wet

microbursts. Pryor (2005) found that values ≥ 50 are characteristic of wet microburst winds of 35 knots or larger. While the MDPI is currently being used operationally by 45 WS forecasters, the WMSI is a more modern wet microburst forecasting tool and has not been tested for the KSC/CCAFS complex.

2) FORECASTING TOOL VERIFICATION

A common method for assessing forecast skill of binary forecasting aids (i.e. to forecast yes or forecast no) such as MDPI or WMSI is the 2 X 2 contingency table (Wilks 2005). Such a table is provided in Table 4. For instance, the number of times an event did occur and was also predicted to occur is given by letter "a" in Table 4. The use of the letters "a,b,c,d" in Table 4 can be used to calculate forecasting skill attributes such as the Probablility of Detection (POD), False Alarm Ratio (FAR), Critical Success Index (CSI), and Heidke's Skill Score (HSS) (Wilks 2005). These relationships are given by Eqs. (3)-(6) below in terms of "a,b,c,d":

Table 4. 2x2 contingency table.

		Observed	
		Yes	No
Predicted	Yes	a	b
	No	c	d

$$\frac{a}{a+c} = POD \tag{3}$$

$$\frac{b}{a+b} = FAR \tag{4}$$

$$\frac{a}{a+b+c} = CSI \tag{5}$$

$$\frac{2 \cdot (ad - bc)}{(a+c)(c+d) + (a+b)(b+d)} = HSS \tag{6}$$

The POD (Eq. (3)) simply describes the probability of successful yes forecasts (i.e. when a forecasted event is observed to occur) for any index. The FAR describes how likely an index will issue a "false alarm." Put another way, the FAR defines the probability of yes forecasts that are found to not occur. Unlike POD, FAR has an inherent negative orientation. That is, lower values of FAR are considered desirable with higher FAR values deemed undesirable. Thus an ideal forecasting index is one with a high POD and low FAR. The CSI, also known as the Threat Score (TS), is a ratio that describes the number of correct yes forecasts to the number of times an event was forecast and/or observed. Values of CSI range between 0 and 1, with a perfect CSI score being 1. The HSS, shown in simplified form by Eq. (6), is a forecast skill statistic that assesses skill with respect to "reference forecast accuracy." The reference forecasts that HSS uses are forecasts that are made by pure chance. HSS values can range between -1 and 1. Forecasts that are found to be better than the reference

forecasts receive positive (but less than 1) HSS scores. Forecasts found to be *worse* than the reference forecasts receive negative (but not less than -1) HSS scores. Forecasts deemed to be exactly as skillful as the reference forecasts receive an HSS score of zero.

Each of these forecast skill scores will be calculated for both MDPI and WMSI for several breakouts. A general forecast skill evaluation will be used to assess general skill characteristics of MDPI and WMSI. Two other breakouts will be included. To determine if either index performed better or worse in any given month, a monthly forecast skill evaluation will be conducted. Finally, a forecast skill evaluation will be performed using the definitions of various flow regimes as described in Lericos *et al.* (2000) and were used in a recently developed Florida lightning climatology that is being used operationally by the National Weather Service Melbourne, FL and the 45 WS. These flow regimes are listed in Table 5.

3) Evaluation of other RAOB convective wind gust forecasting tools

Because the convective wind forecasting problem includes both the likelihood of convective winds and the predicted peak wind gust associated with these events, an error evaluation of four convective wind gust forecasting tools was also performed. For the purposes of the error evaluation, the maximum surface peak wind speed (in knots) was compared to the predicted gust for each RAOB wind gust prediction technique.

Three convective wind gust forecasting tools were evaluated. The first gust prediction method, devised by McCann (1996), was the Wind Index (WINDEX). The WINDEX is represented mathematically by the following:

$$WINDEX = 5 \cdot \sqrt{H_m \cdot R_q \left(\Gamma^2 - 30 + Q_l - 2 \cdot Q_m \right)} \quad (7)$$

Where H_m is the height of the melting level (in km), Q_l is the mean mixing ratio (in g kg^{-1}) from the surface to 1 km, R_q is Q_l divided by 12, Q_m is the mixing ratio (in g kg^{-1}) at the freezing level, and Γ is the surface to freezing level lapse rate (in°C km^{-1}). The last three indices are convective wind gust forecasting tools

Table 5. Definitions of flow regimes. Adapted from Cummings *et al.* (2007)

FLOW REGIME	SUBTROPICAL RIDGE POSITION
SW-1	Subtropical ridge south of Miami
SW-2	Subtropical ridge between Miami and Tampa
SE-1	Subtropical ridge between Tampa and Jacksonville
SE-2	Subtropical ridge north of Jacksonville
NW	Subtropical far to south and extending far in Gulf of Mexico and stronger than normal
NE	Subtropical far to north and extending into SE US and much stronger than normal
Other	Subtropical ridge position not defined

developed by the Air Force (Miller 1975) and are referred to as the Synder Method, and the T1 and T2 methods. Once a wind gust is derived from the T1 method, an environmental wind speed correction (the mean wind speed from the surface to 5000 ft) is added to obtain the true gust. After T2 is calculated, three values are provided: a minimum expected gust speed, an average gust speed,

and a maximum gust speed. Instead of using a range, the maximum gust speed is used for the T2 gust speed.

Two commonly used statistical measures of forecast error are the root-mean-square error (RMSE) and the mean absolute error (MAE). These equations are:

$$RMSE = \sqrt{\frac{1}{n} \cdot \sum_{k=1}^{n} (y_k - o_k)^2} \tag{8}$$

$$MAE = \frac{1}{n} \cdot \sum_{k=1}^{n} |y_k - o_k| \tag{9}$$

In Eqs (8)-(9), y_k is the k^{th} predicted value and o_k is the k^{th} observed value in some arbitrary dataset of size n, RMSE is the root-mean-square error (in kt) and MAE is the mean-absolute error (in kt). The advantage of using the MAE is that because the error term is squared in the RMSE equation, the RMSE can be quite large in situations when the error for only a few cases is large. Sullivan (1999), in an evaluation of predictive gust equations using Doppler radar information, defined a "hit" as those cases in which the predictive method correctly guessed the convective wind gust to within +/- 5 knots of accuracy. In addition to the RMSE and MAE, the number of "hits" will also be compiled for WINDEX, T1 and T2 RAOB gust forecast predictions. A large number of "hits" implies reasonably good forecast accuracy.

4) Development of threshold theta-e lapse rates for convective wind warning decisions

Once a theta-e lapse rate equation was devised, a procedure that is referred to as Relative Operating Characteristics (ROC) was applied to the theta-

e lapse rate values that are computed. The ROC procedure (Wilks (2005)) uses a graph of the Probability of Detection on the y-axis and the False Alarm Rate on the x-axis. Threshold values of theta-e lapse rate may be found by starting from the lowest theta-e lapse rate encountered in the dataset and then incrementing these by some arbitrary value (in this case, .5 K km^{-1} will be used as the increment). Plotting and connecting the (FAR, POD) ordered pairs for each theta-e lapse rate value will result in a curve. From this curve, an "optimal value" (i.e. that value that best maximizes POD and minimizes FAR) can be selected as an appropriate threshold for warning decisions. ROC diagrams will be constructed for each of the flow regimes defined in Lericos *et al.* (2000).

c. WSR-88D Doppler radar techniques data and methodology

This section will discuss the data and methodology associated with convective wind forecasting techniques associated with WSR-88D Doppler radar data. Many of the assumptions mentioned in Section 2 would also apply here.

1) DOPPLER RADAR DATA

Each of the Doppler radar-measured quantities was obtained from a file referred to as "Storm Structure" from the National Climatic Data Center (NCDC) KMLB (Melbourne, FL) Doppler radar archives. This file is an alphanumeric, tabular product that is generated by the Storm Cell Centroid Sub-Function (SCCS), one of the four major sub-functions in the Storm Cell Investigation and Tracking (SCIT) algorithm. This product relays information on the following storm cell attributes, updated at each successive volume scan:

- Cell-based Vertically Integrated Liquid (VIL) (kg m^{-2})
- Azimuth and Range of storm cell from RDA (in degrees)
- Cell Base and Echo Top (in kilofeet)
- Maximum Reflectivity (in dBZ)
- Height of the Maximum Reflectivity (in kilofeet)

Each of these parameters are computed for each storm cell, which are given an alphanumeric "name" or "ID" (such as "J8", for example), with each storm ID being ranked according to cell-based VIL. One final parameter that was computed from the Echo Top and the Cell Based VIL is the VIL Density. This is defined mathematically in Eq. (10) as:

$$VILDensity = \frac{VIL}{ET}, \tag{10}$$

where VIL is the cell-based VIL (in kg m^{-2}), ET is the Echo Top (in kilofeet), and VIL Density is the VIL Density (in kg m^{-3}). .

The approximate time of the convective wind gust was documented for each event. The latest Storm Structure datafile corresponding to the approximate time of the convective gust was then taken for each case day from the NCDC Melbourne, FL (KMLB) WSR-88D Level III data archive.

Two problems were encountered when collecting the storm cell attributes. The first problem pertained to the selection of the storm cell that likely generated the convective gust. To mitigate this problem, the KSC mesonetwork tower to which the maximum gust occurred was noted. By using Figure 1, which displays the various towers in the KSC mesonetwork, the closest cell ID to the location of the tower was used. The second problem came about as a result of the radar

beam not being able to detect the exact echo top height. In a small minority of the episodes chosen, an estimate of the echo top height was given for some cells—typically reported as greater than some specified height. The most likely cause for this is probably due to the actual cell top height being too high for the radar to measure. For these cases, only this specified height (i.e. the height that the radar beam could reasonably assume was the height of the cell) was used as that cell's echo top. This effectively truncated the cell top height of some of the cells to this minimum cell top height.

2) CORRELATIONS OF RADAR VARIABLES TO OBSERVED KSC GUSTS

Several studies, as described in Chapter 1, have described various base reflectivity and / or radial velocity signatures characteristic of microbursts. It may also be of interest to show which of the variables in Section 3(b) are best correlated to KSC convective wind speeds. Tables of calculated R^2 values to the observed KSC gust for each parameter in Section 3(a) will be provided. These correlation statistics may reveal qualitative assessments as to which of the three equations in Sullivan (1999) may work well as forecasting aids.

3) EVALUATION OF THE ECHO TOP / VERTICALLY INTEGRATED LIQUID EQUATION

As mentioned in Chapter 1, Sullivan (1999) performed an initial error evaluation of three predictive wind gust equations for the KSC/CCAFS complex using WSR-88D data for 15 warm-season microbursts. Because of the limited dataset, Sullivan suggested that his findings may not be conclusive. This thesis will update Sullivan (1999) using just the Echo Top/Vertically Integrated Liquid

wind gust potential equation (ET/VIL), but for a 44-sample dataset of wind speeds—30 warning-criteria wind speeds and 14 below-criteria wind speeds.

The ET/VIL relationship based from theoretical work done by Emanuel (1981), and was mathematically derived by Stewart (1996), as follows:

$$w = \sqrt{\left(20.628571 \cdot VIL\right) + \left(-3.125 \times 10^{-6} \cdot ET^{2}\right)} \qquad (11)$$

Where VIL is the cell-based VIL (in kg m^{-2}), ET is the Echo Top (in kilofeet), and w is the maximum predicted downdraft speed (in m s^{-1}).

The same statistical error parameters that were used by Sullivan (1999) to evaluate the RAOB wind gust forecasting tools (i.e. RMSE, MAE and number of "hits") were recomputed using the larger dataset and then compared with Sullivan's results for the ET/VIL equation.

4) Additional radar techniques

Recall from Chapter 1 that several studies (Proctor 1989; Srivastava 1987; Atlas *et al.* 2004) have shown that the precipitation type that falls out of a convective cloud is important in determining whether or not wet microburst generation occurs. More specifically, the above authors found that meltwater from hailstones are required for microbursts to form in weakly unstable lapse rate environments. Those findings will be tested using the 44-case dataset described above. The height (in kilofeet) and value (in dBZ) of the maximum radar reflectivity prior to convective wind onset—taken from the "Storm Structure" datafile as mentioned previously--will be compared to the observed height of the

freezing level. Freezing level data (in units of kilofeet) will be taken from the most recent XMR RAOB. The assumption implied here is that storms with maximum reflectivity cores above the freezing level have a greater potential to produce hailstones (and following the research findings from the authors previously mentioned, wet microbursts), especially if the associated reflectivity value is also sufficiently high. A graph showing the difference in height between the max reflectivity height and height of the freezing level, the max reflectivity value, and the associated KSC wind gust was created to show if these previous research results apply to forecasting KSC/CCAFS convective wind episodes.

Using MATLAB statistical software, a multiple linear regression model was built that uses the storm cell attributes as predictors. The predictors were selected using forward selection procedures. Significance of this new model will be tested with an ANOVA table F-test, and an assessment of the normality of the regression residuals. To assess its potential as a future operational tool, this equation was tested against a 22-case dataset, independent from the 44 cases that were used in its development. The 22-case dataset includes both below criteria wind speeds and above warning-criteria wind speeds. Similar error statistics computed for the ET/VIL equation will be computed for this new equation so that comparisons can be made.

CHAPTER 3

1. Verification of existing RAOB-based forecasting tools

a. Climatological frequencies of warning-level convective wind gusts

Before discussing the evaluation results of the various forecast tools that use radiosonde data as input, it is prudent to provide some background as to how often the ≥ 35 kt peak convective winds occur at KSC/CCAFS.

Figure 5 shows the warm-season monthly climatology of convective wind occurrences. This figure shows the lowest and the highest number of days that any convective wind speed occurred for each month in any of the 11 years that comprise the convective wind climatology. Also shown here is the average number of convective wind days for each month (shown in the red bars on Figure 5). From the figure, it can be shown that the average number of occurrences of any convective wind speed reaches a maximum in August, and the average reaches a minimum in May. It was shown in Koermer and Loconto (2005) that the monthly climatology of warning-level convective winds follows a normal distribution, with the peak centered around July and with minima in May and September.

Figure 6 shows the distribution of convective wind speed occurrences by synoptic flow regime as characterized by Lericos *et al.* (2000) and defined in Chapter 2. Also shown in Figure 6 is the average peak convective wind speed in that particular flow regime. From the figure, it is observed that not only are westerly flow regimes favored for convective winds, but the westerly flow regimes are also characterized as having higher mean peak convective wind speeds.

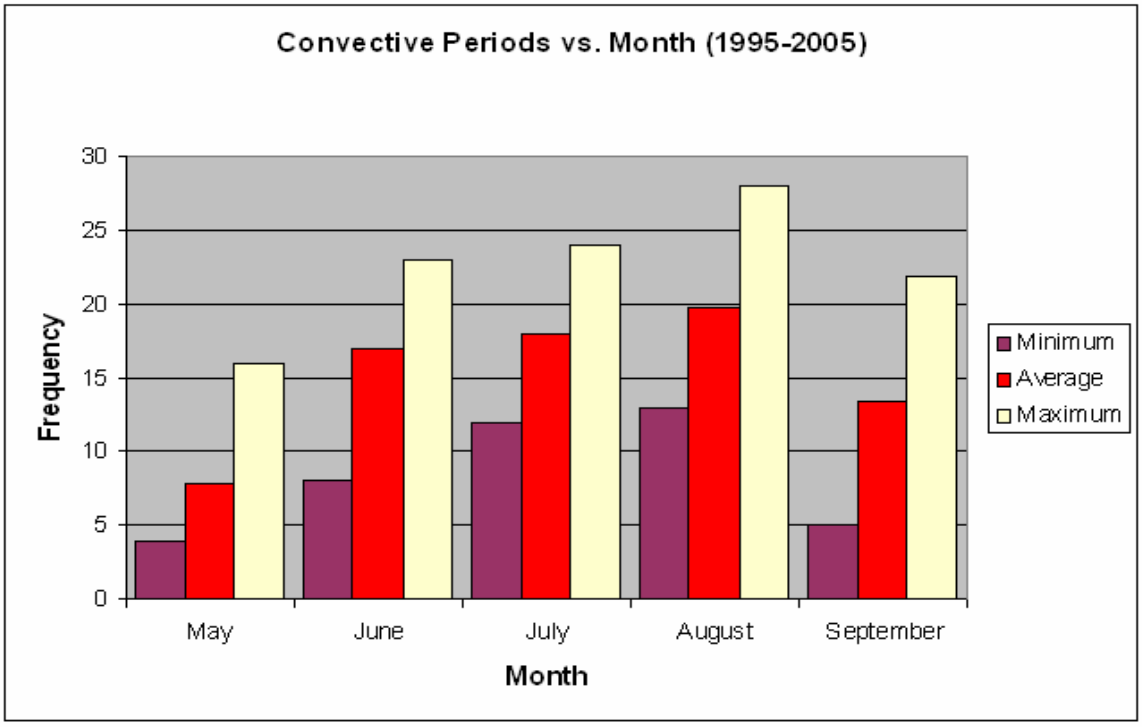

Figure 5. Monthly climatology of all convective winds at KSC/CCAFS. Adapted from Cummings *et al.* (2007).

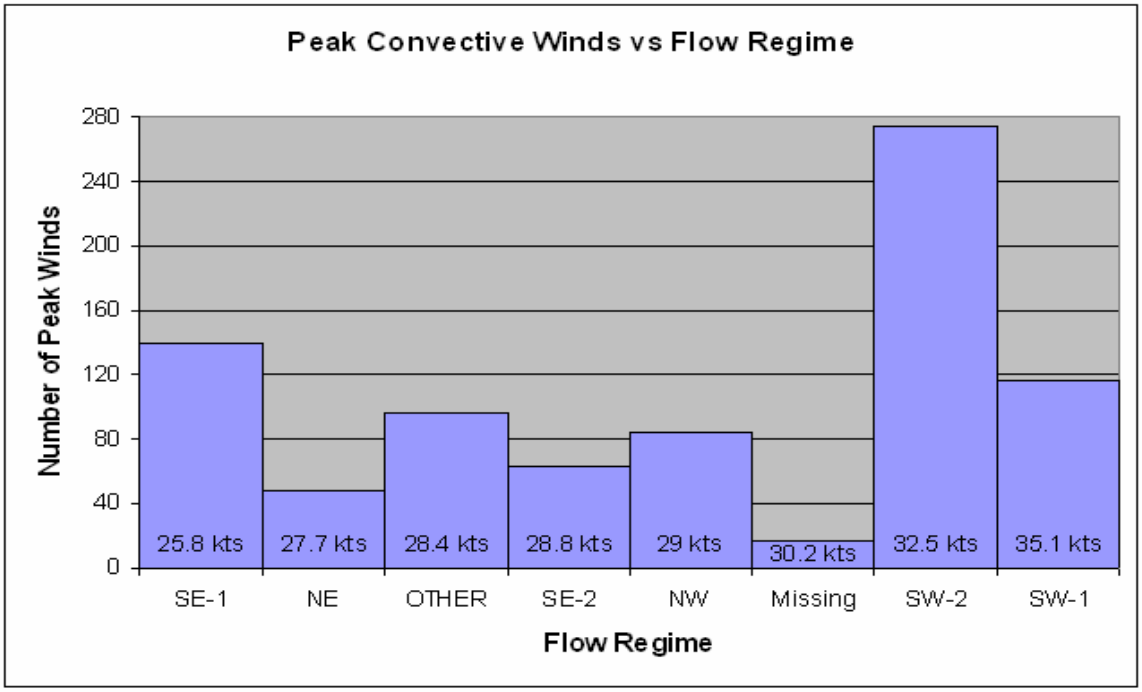

Figure 6. Distribution of all convective wind speeds by flow regime. Adapted from Cummings *et al.* (2007).

Figure 7 shows the number of peak convective wind speeds separated into 5-knot convective wind speed categories. The distribution of peak convective winds over the 11 year climatology follows an approximate Gumbel cumulative probability function. The curve of this distribution is shown in green in Figure 7. The general trend is that higher peak wind speeds tend to decrease in occurrence from the peak wind speed occurrence maximum of between 20-24 knots.

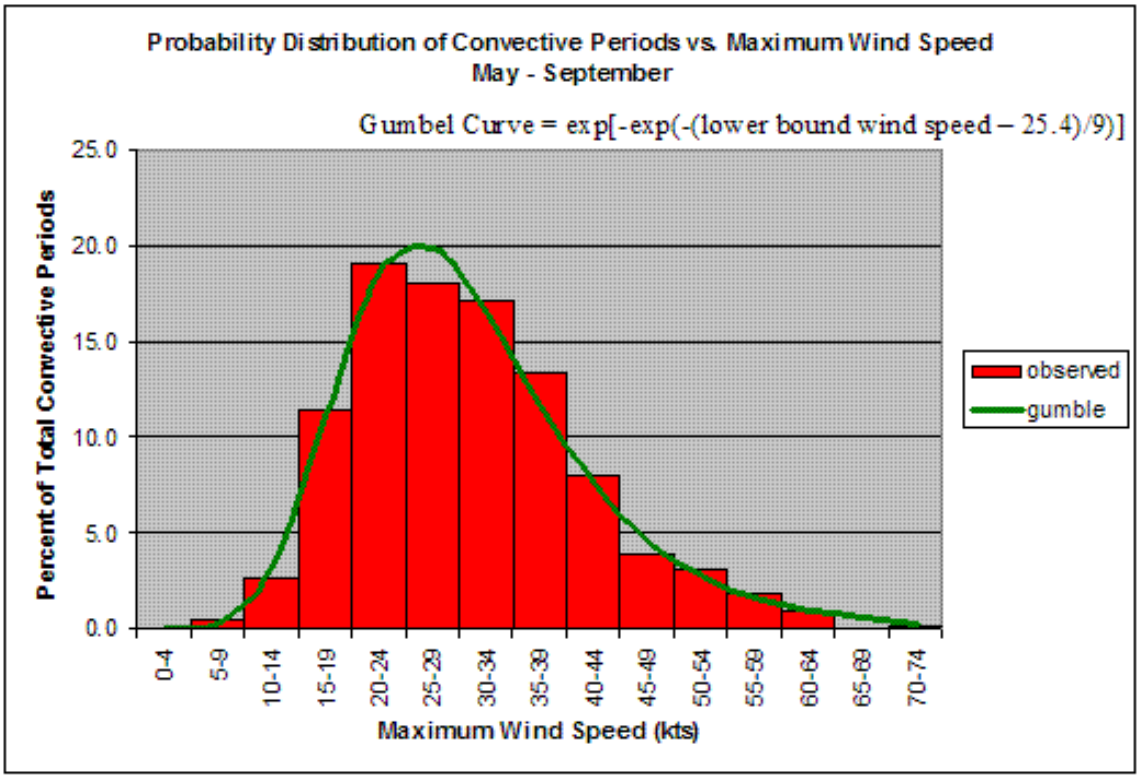

Figure 7. Distribution of peak convective wind speeds by wind speed category. Adapted from Cummings *et al.* (2007).

Integration under this Gumbel equation for some arbitrary lower-bound wind speed to infinity will yield specific probabilities of various convective wind

speed ranges. For instance, integration under the curve provides a probability of .31 for ≥ 35 knot convective winds. Put another way, according to the Gumbel fit, warning-level convective winds occur just less than one-third of the time. Less frequent probabilities are discovered for ≥ 50 knot wind speeds and ≥ 60 knot wind speeds, with probabilities of .07 and .02, respectively, for these more severe wind speed categories.

b. General forecasting verification of MDPI and WMSI

Figure 8 shows the various forecasting verification metrics for both MDPI and WMSI. The two forecast indices appear to be quite similar in terms of the various forecasting verification indicators. For both indices, the WMSI and MDPI both predict a positive warning-level wind detection and false alarm at roughly the same probability (about 50%). It does appear that MDPI is a slightly better index, but the high false alarm rates for both indices suggest that neither MDPI or WMSI are reasonably reliable forecasting aids.

c. Forecast verification of MDPI and WMSI by synoptic flow regime

The next two sections will show the evaluation of the Microburst Day Potential Index (MDPI) and Wet Microburst Severity Index (WMSI) by synoptic flow regime.

1) MICROBURST DAY POTENTIAL INDEX

Figure 9 shows a bar graph of the various forecast skill scores defined in Chapter 2 as applied to MDPI as a function of flow regime. Recall that an ideal index is one that has a POD of near 1 and a FAR of near zero.

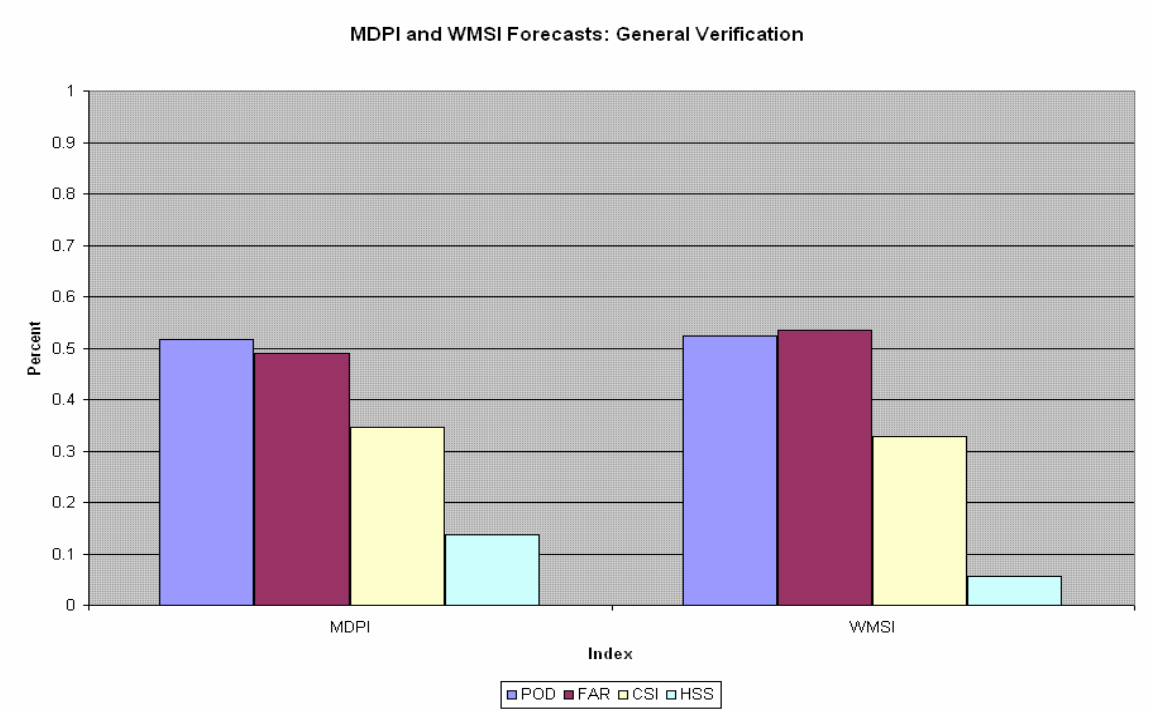

Figure 8. General forecast verification for MDPI and WMSI.

Examination of Figure 9 shows that the MDPI forecasts warning-level convective wind speeds that occur under the SW-2 flow regime relatively well, with a POD of just above .60 and a FAR that is slightly less than .30. However, for most of the other flow regimes, the FAR is undesirably quite high, with values reaching higher than .50. In some regimes (Missing, NE, NW, and SE-2), we find for these regimes that the Heidke's skill score is negative, implying that the MDPI has worse forecast skill than random chance forecasting.

2) WET MICROBURST SEVERITY INDEX

Figure 10 shows the same bar graph as Figure 9 but for the WMSI. Based on the figure, similar results are found for WMSI as observed for MDPI. The only flow regime that WMSI will forecast warning-criteria winds reasonably.

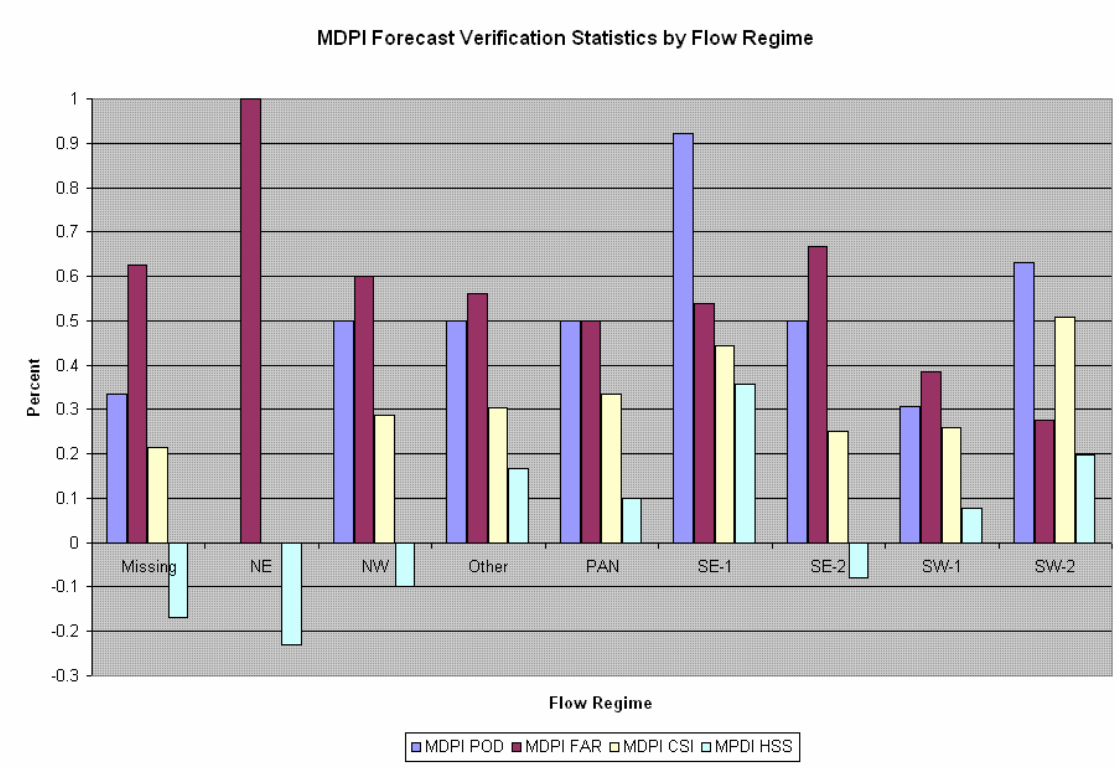

Figure 9. MDPI forecast verification statistics by flow regime.

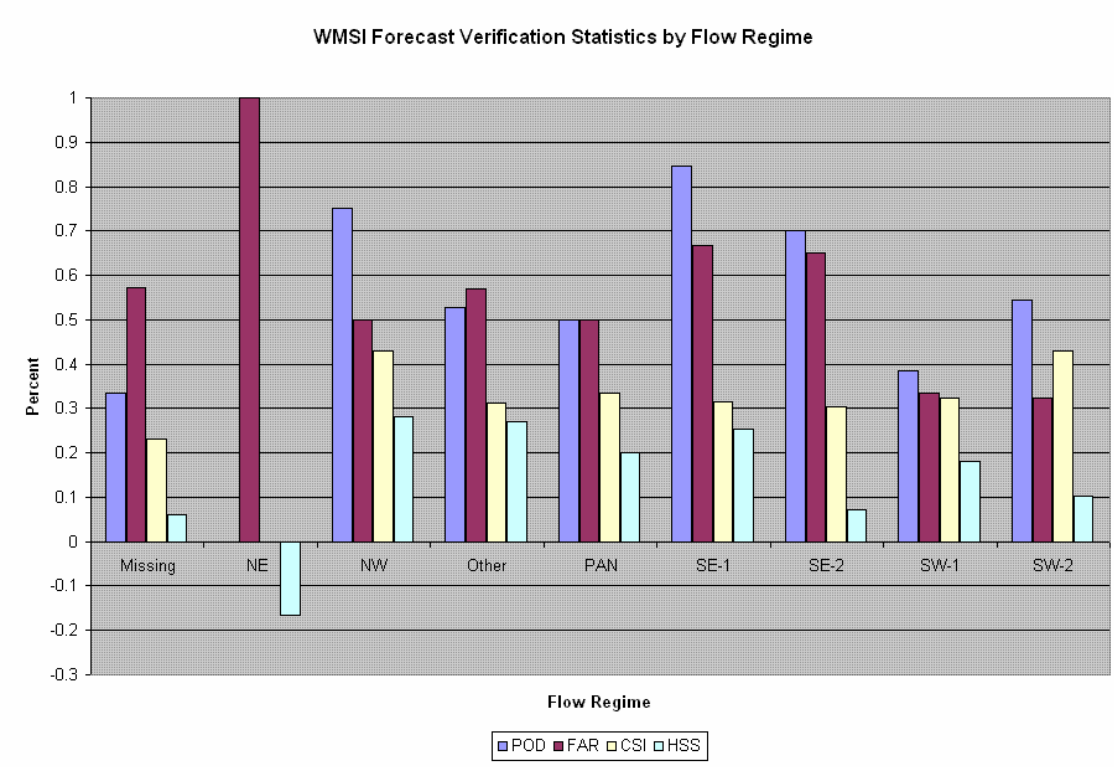

Figure 10. As in Figure 9, but for WMSI.

It is also observed that exceedingly high FARs for the other flow regimes make this index also an ineffective forecasting tool for these other regimes.

d. Monthly forecast verification of MDPI and WMSI

To assess potential monthly skill in MDPI and WMSI, the following sections will show forecast verification statistics of MDPI and WMSI by month.

1) MICROBURST DAY POTENTIAL INDEX

Figure 11 shows the verification metrics computed for MDPI by month. This figure shows that the general trend is for MDPI to perform better as the warm season gets later and later. Excluding the month of September, for MDPI the POD increases modestly as the FAR decreases. It best forecasts warning-level episodes in the month of August. Generally speaking, MDPI forecasts monthly occurrences of warning-level gusts only adequately at best.

2). WET MICROBURST SEVERITY INDEX

Figure 12 shows the forecast verification for WMSI. The general trend for WMSI is that from May through August, both the POD and FAR increase linearly, while decreases in POD and FAR are noted in September. The May CSI value is actually quite high (nearing a value of .6), while both POD and FAR for these are low. The CSI quantifies how successful an index is at predicting “rare” events (i.e. when event non-occurrence occurs more frequently. There are two possible reasons for this result—the number of May events is low, and as implied by the low FAR, that the number of false alarms is also a low value. Referring back to Eq. (5) in Chapter 2, the combination of these two factors results in the denominator of Eq. (5) being small (values for b and c are small).

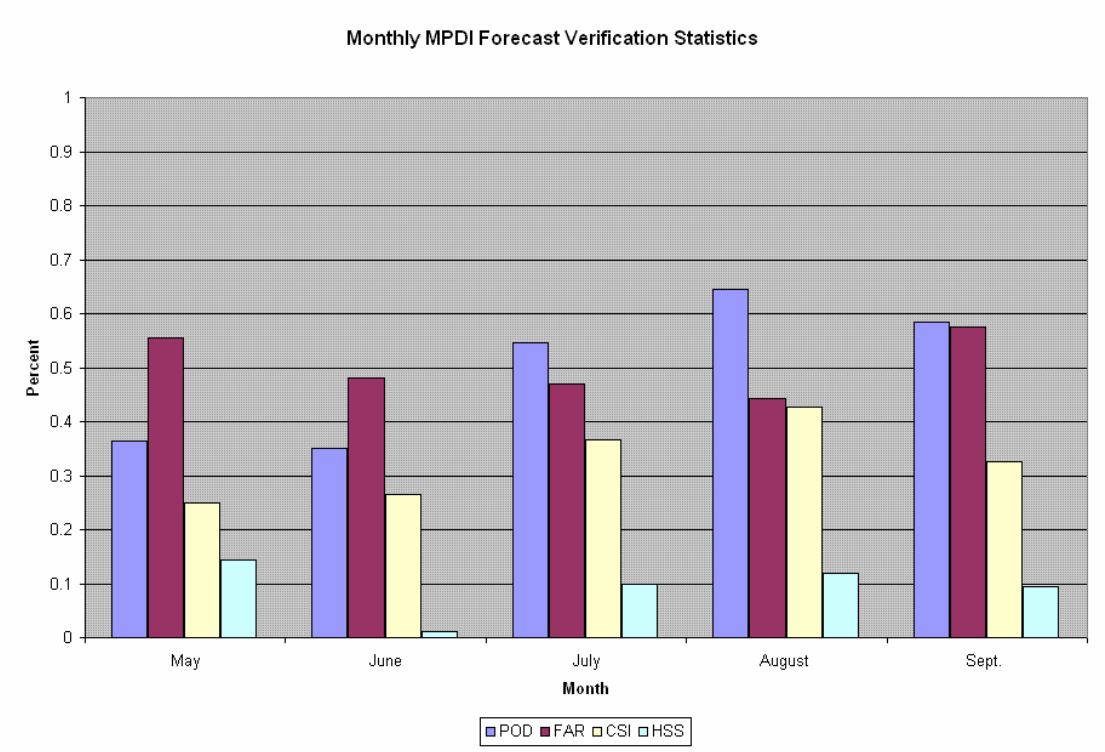

Figure 11. MDPI forecast verification stratified by month.

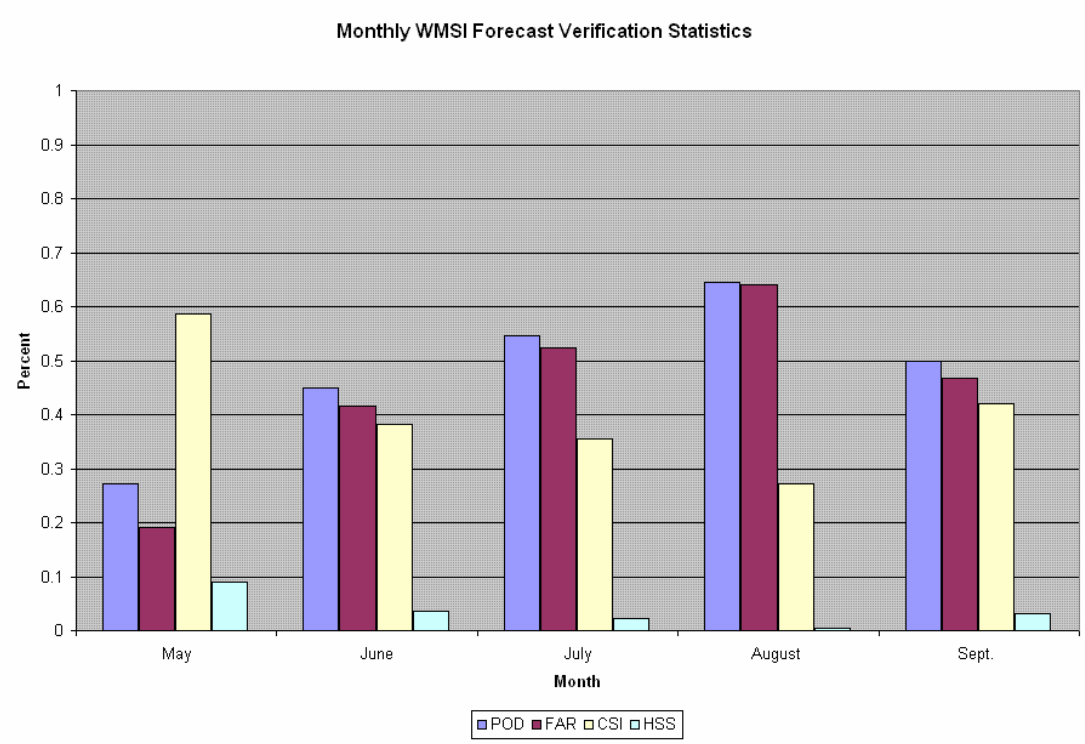

Figure 12. As in Figure 11, but for WMSI.

e. Error evaluation of RAOB-based peak convective wind gust predictors

This section will show the results of the error evaluation of the four peak convective wind gust forecast predictors (i.e. WINDEX, Snyder Method, T1 and T2).

Figure 13 plots the predicted wind gust speeds from each of the various techniques versus the observed convective wind gust measured from the KSC mesonetwork. From the figure, as expected, none of the four indices that were evaluated predicted the observed peak gust (shown by the dark blue line) with any consistency. The T1 and the Snyder Method have two biases that are evident from the figure. The T1 (pink curve) has a marked high bias, while the Snyder Method has a low bias. The Snyder Method might have a low bias because of the fact that one of the terms in its computation involves adding the mean wind speed 5,000 ft above and below the Wet Bulb Zero height.

Because wind speeds during the Florida warm-season are light, this term in the Snyder Method is low. For the severe winds (≥ 50 knots) the techniques generally underpredict the peak gust. The T1 does appear to do an adequate job at predicting the gusts for these events, but this is more likely because of its high Meanwhile, for winds speeds less than 50 knots or so, excluding the Snyder Method, a general overestimate of the observed wind is noted from the techniques. An error table the shows the RMS error, Mean Absolute error and number of hits is shown in Table 6. It can be inferred qualitatively from Figure 13 that there does not appear to be any significant correlation between the observed convective wind speeds and the peak speed as predicted from any of the four

methods evaluated. This is supported quantitatively by Table 7, which summarizes the correlations between the observed peak gust and the predicted gust by T1, T2, WINDEX or the Snyder Method, as values are very close to zero.

Table 6. RAOB wind gust error table.

	T1 Gust	T2 Gust	Snyder	WINDEX
RMSE	14.81041	8.791783	20.7075	10.47259
MAE	12.01713	7.340909	18.4596	8.49495
Hits	14	18	5	14

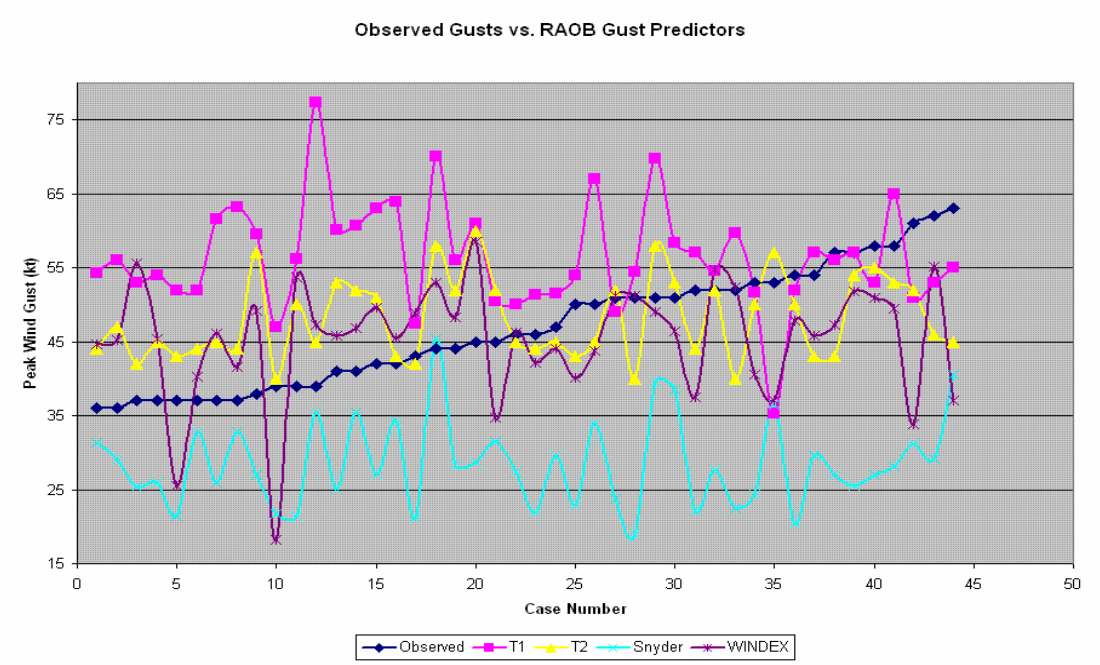

Figure 13. Line scatterplot of predicted wind speeds from T1, T2, Snyder Method and WINDEX versus observed peak gust.

Table 7. Correlation between observed gusts and predicted gusts for each RAOB gust prediction technique.

Technique	Correlation
T2	0.0349
T1	0.0249
WINDEX	0.0113
Snyder	0.0005

CHAPTER 4

4. Evaluation OF WSR-88D Doppler radar forecast tools

a. KSC peak convective wind speeds versus various storm cell attributes

Figure 14 shows a scatterplot of the peak convective wind speed measured at KSC versus values of cell-based VIL for each of the 44 convective wind episodes included in the radar study. Recall that 30 of these episodes had warning-criteria wind speeds and that 14 had below warning-criteria wind speeds. Subjectively speaking, there does appear to be a linear relationship between the two quantities. Most of the weaker convective wind speeds (i.e. those between 19 and 40 knots) tend to have cell-based VIL values ranging between 10-15 kg m^2. Values of cell-based VIL above 20 kg m^2 appear to characterize strong to severe wind speeds of ≥ 45 knots, while cell-based VIL values above 35 kg m^2 are almost exclusively associated with wind speeds exceeding 50 knots. High values of cell-based VIL are characteristic of strong thunderstorms, ones that are likely to exhibit intense rainfall and/or the presence of hail.

Figure 15 shows a scatterplot of the peak KSC wind gusts versus Echo Tops (in thousands of feet). There does not appear to be as strong of a linear correlation between these two variables as was shown with cell-based VIL. In general, a good majority of the cells that produce warning-criteria wind speeds have echo tops of ≥ 29,000 ft. Nearly all below-criteria wind gusts (and a few above-criteria wind episodes) occur with echo tops less than this value.

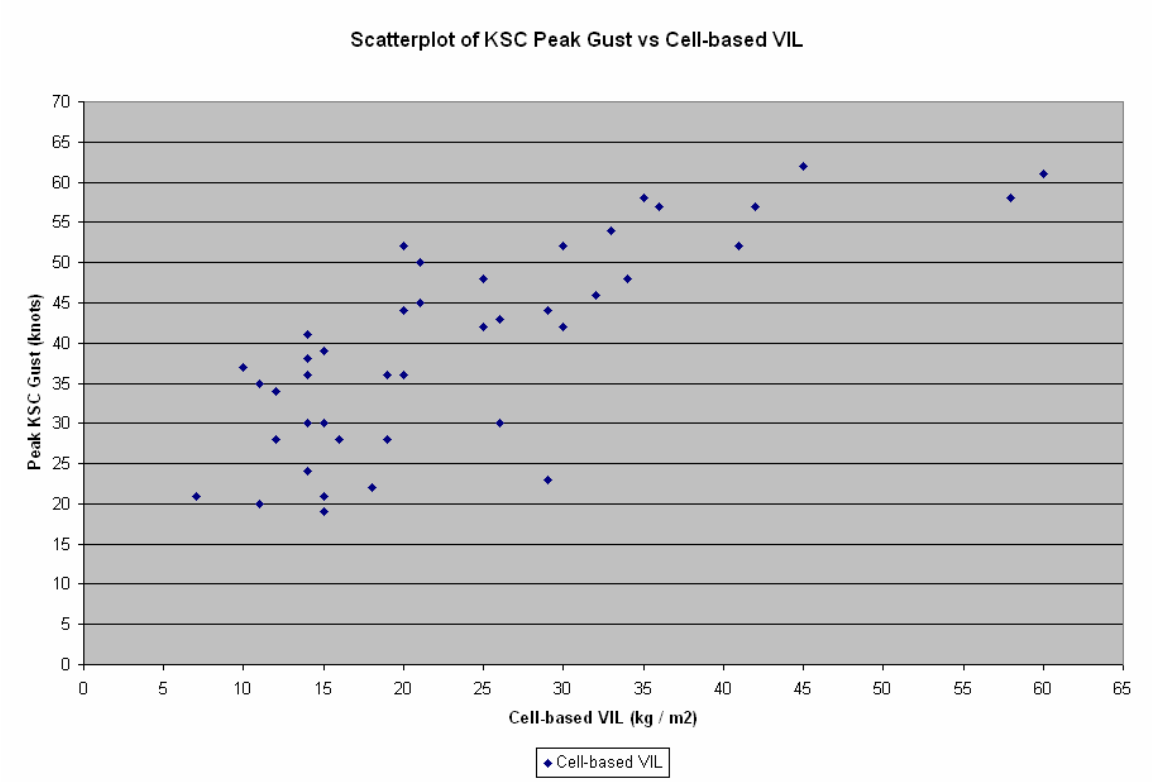

Figure 14. Scatterplot of peak KSC wind gust vs. Cell-based VIL.

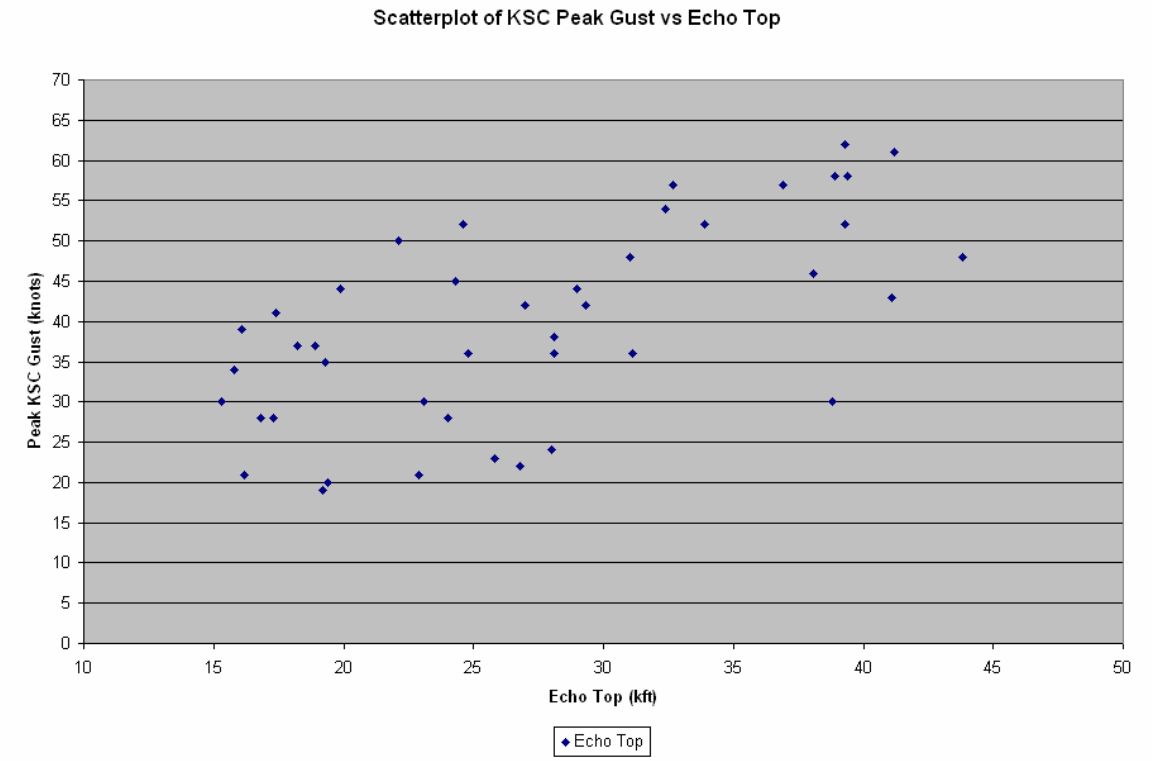

Figure 15. As in Figure 14, but for echo tops.

Since VIL and the Echo Top are used to derive the VIL Density parameter, it seems appropriate to show the scatterplot of VIL Density versus KSC peak wind gusts. This is shown in Figure 16. There does appear to be a fairly good linear relationship between VIL density and peak KSC wind gusts for warning-level events, but below-criteria events can have values ranging from around 1.3 kg m^3 to near 3.7 kg m^3, resulting in a weaker correlation for VIL density for all wind speeds.

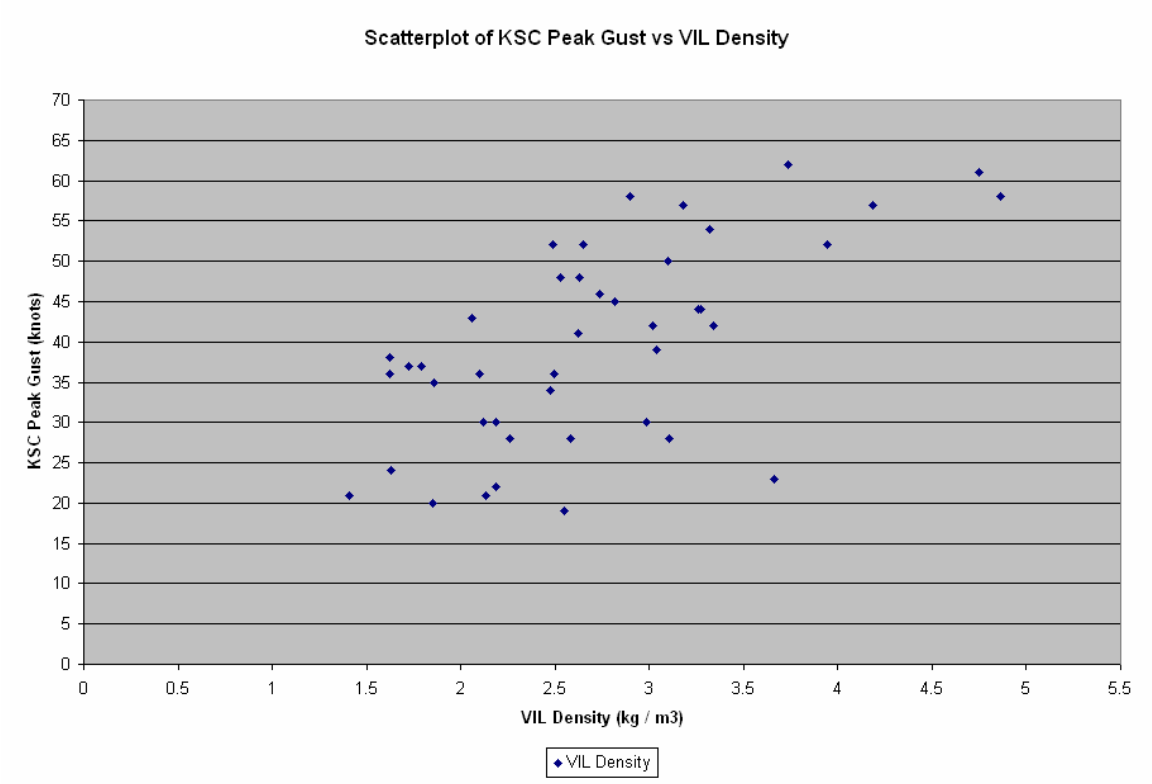

Figure 16. As in Figure 14, but for VIL density.

The wide variation in VIL density values for below-criteria wind events is probably more due to variations in cell echo top than in cell-based VIL. Because for most cases values of cell-based VIL for below-criteria wind cases is generally

small (~10-15 kg m^2, from Figure 14), under these conditions a less vertically-developed storm (generally characteristic of below-criteria events from Figure 15) would still yield a potentially large value of VIL density. Taking this into account, it can be seen from Figure 16 that values of VIL density that exceed 2.5 kg m^3 are more likely to be associated with warning-level wind speeds.

A scatterplot between peak KSC wind gusts and values of peak reflectivity is shown in Figure 17. There does appear to be a fairly good correlation between the peak KSC wind gust and the value of maximum reflectivity. Most of the below-criteria wind episodes are associated with maximum reflectivities less than about 55 dBZ. Cells that have maximum reflectivities above about 58 dBZ are generally characteristic of cells with severe wind speed potential (exceeding 50 knots). Maximum reflectivity values this high would seem to be necessary to maintain the very intense rain shafts that accompany wet microbursts; however, values this high also might indicate the presence of hailstones in the convective cloud.

Figure 18 shows the scatterplot of KSC peak convective wind speeds versus the height of the maximum reflectivity. From the figure, the relationship between the peak convective wind speed and the height of maximum reflectivity is weak. Most of the wind speeds ≥ 45 knots have max reflectivity heights generally above 15,000 ft. It is difficult to pinpoint a value that would best differentiate between above-criteria wind speeds and below-criteria episodes, but a value of ≥11,000 ft would probably best fit this value.

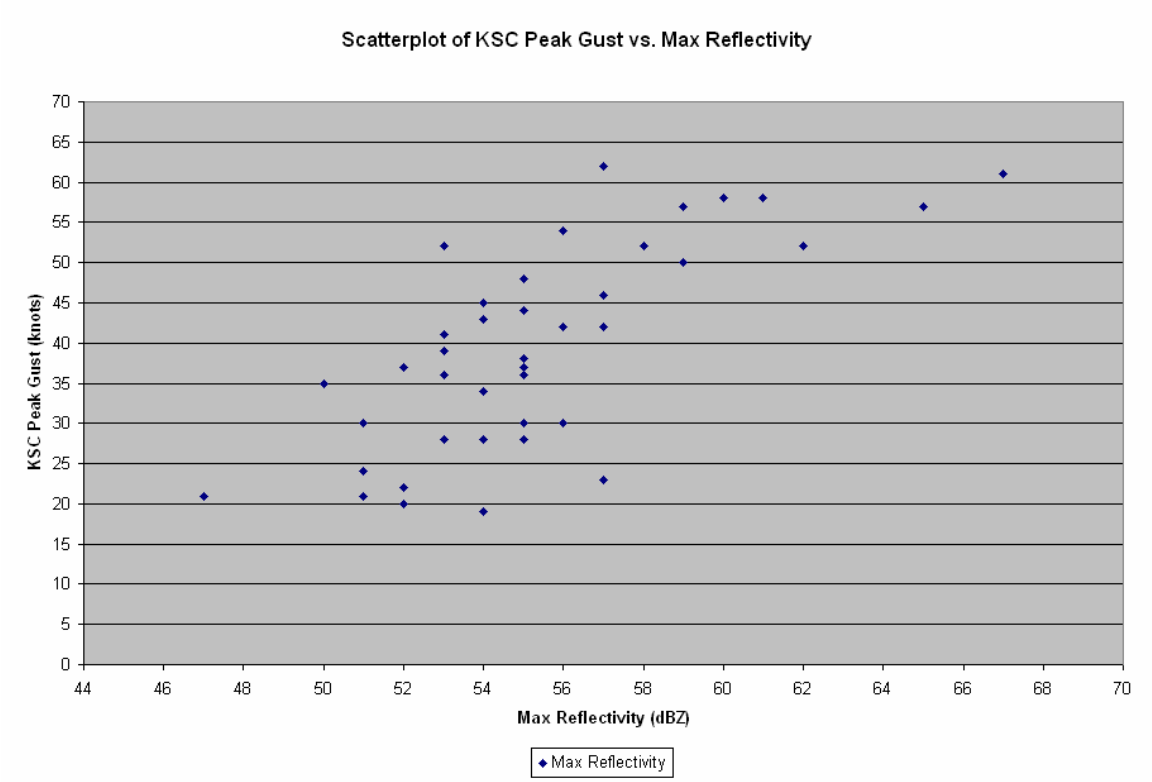

Figure 17. As in Figure 14, but for maximum reflectivity.

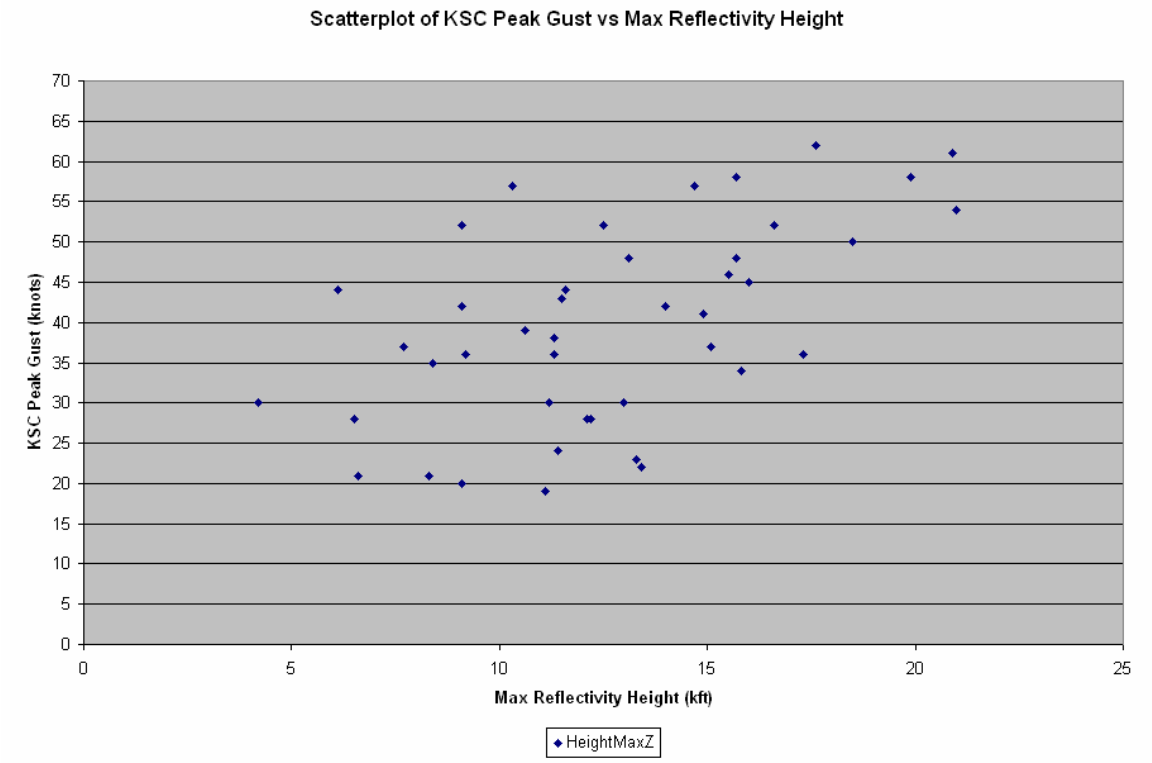

Figure 18. As in Figure 14, but for max reflectivity height.

Table 8 shows the correlation statistics between the variables previously described and the peak KSC convective wind speed. The general subjective descriptions of the strength of the linear relationship between the various cell attributes and the peak KSC wind gust from the individual scatterplots are verified quantitatively in Table 8. Based on the table, and on the previously shown figures, cell-based VIL and maximum reflectivity are the best correlated variables.

Table 8. Correlation statistics table.

Cell Attribute	**Correlation**
Cell-based VIL	0.5806
Max Reflectivity	0.5123
Echo Top	0.4067
VIL density	0.3979
Height Max Z	0.3108

b. A possible relationship between peak KSC convective winds and hail potential

As shown in the previous section, it was found that the values of cell-based VIL and maximum reflectivity were best correlated to the observed KSC peak convective wind gust. The fact that these two predictors were best correlated is interesting in the sense that both parameters are also potential indicators of the presence of hail, and as shown in Chapter 1, several authors have specified through the results of modeling studies that hailstones be present for melting to produce wet microbursts in stable temperature lapse rate environments.

To further research these findings for potential operational significance, Figure 19 was constructed. This plots both the value of maximum reflectivity (shown by the dark blue line which follows the right y-axis) and the difference in height in kilo-feet between the height of maximum reflectivity and the RAOB-obtained freezing level height (shown by the light blue bars associated with the left y-axis, with positive height differences indicating reflectivity heights above freezing level) against the observed wind speed. The assumption here is that cores that lie above the freezing level and associated with very high maximum reflectivity values have a good risk of producing hail. Negative height differences (indicating cell cores whose height falls below the freezing level) are generally characteristic of cells with resulting peak convective wind speeds between 19 and 44 knots. While both low-end above-criteria and below-criteria wind speeds generally have cells with cores that do not approach the freezing level, low-end warning criteria events have slightly higher max reflectivity values. However, for the more significant wind speeds (≥ 45 knots), and in particular for the severe wind gusts exceeding 50 knots, cell cores were found to be tall enough to lie above the freezing level.

Thunderstorms that yielded winds in this severe windspeed range also had much larger values of maximum reflectivity, shown by the large jump in the blue dotted line. Although not shown explicitly here, it can be inferred from Figure 14 in the previous section that high values of cell-based VIL were present for the severe wind gusts. Given these results, combined with those mentioned in the previous section, thunderstorms with a potential to produce hail would also

stand to have a greater chance to produce wind speeds that meet or exceed 45 knots. These results also would lend support to the modeling research results suggested by previous authors.

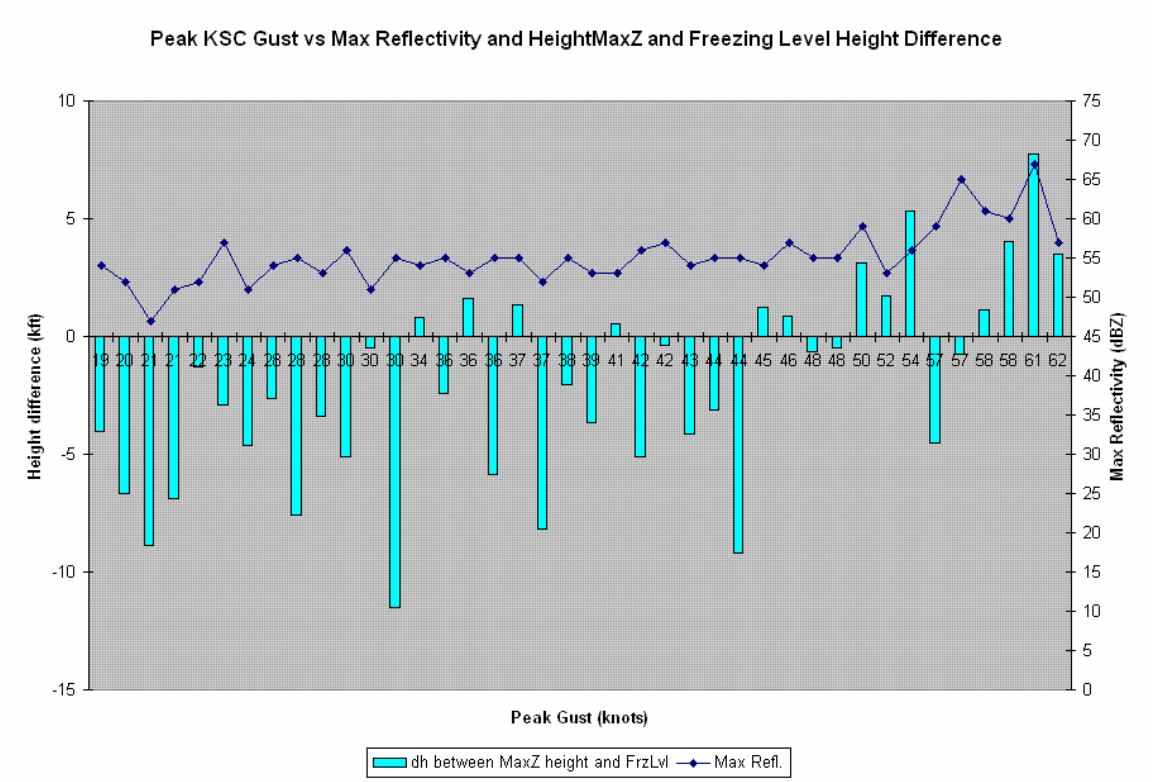

Figure 19. Max reflectivity minus RAOB freezing level height difference, value of max reflectivity versus peak KSC wind gust speed.

c. Evaluation of the Echo Top/VIL Wind Gust Potential Equation

Figure 20 shows a scatterplot of the peak KSC wind gust versus the gust predicted by the Echo Top/VIL gust equation as defined in Chapter 2. The Pearson correlation coefficient is also shown in the figure in order to get a sense of how correlated the two variables are to each other. Based on the figure, a fairly strong positive correlation exists between the predicted gust computed from the ET/VIL wind gust equation and the peak observed value from the KSC

mesonet. Thus, in general, higher values of wind gust speed as predicted by ET/VIL are fairly strongly correlated with increasing values of peak KSC wind speeds, which is what is desirable in comparisons of observed versus predicted wind gust scatterplots.

Figure 21 was created in order to assess any systematic biases in the ET/VIL relationship (i.e. to assess under- or over-forecasts of wind gust speeds). Looking at Figure 21, it appears that the ET/VIL relationship grossly over-forecasts below-criteria convective wind speeds. There is more variability in the plots of warning-criteria wind speeds, with no characteristic under- or over-forecasting bias evident from the figure.

Table 9 show a summary table of various computer error metrics for the ET/VIL relationship, stratified by various wind speed categories. From the table, the ET/VIL will generally predict a thunderstorm's peak wind speed with errors between 6-8 knots.

Larger errors are encountered for below criteria wind episodes, which makes sense given the plot shown in Figure 21, with much less error for above-criteria wind speeds. For using ET/VIL as a guidance tool for issuing convective wind warnings, even though a pretty strong positive correlation exists between ET/VIL predictions and observed gust speeds, the ET/VIL relationship seems poorly suited for accurately differentiating between below-criteria winds and above-criteria wind speeds Although this is unrealistic from a forecasting standpoint, if it is reasonably known in advance that a warning-level gust will occur, the ET/VIL does yield fairly accurate values of peak wind speed.

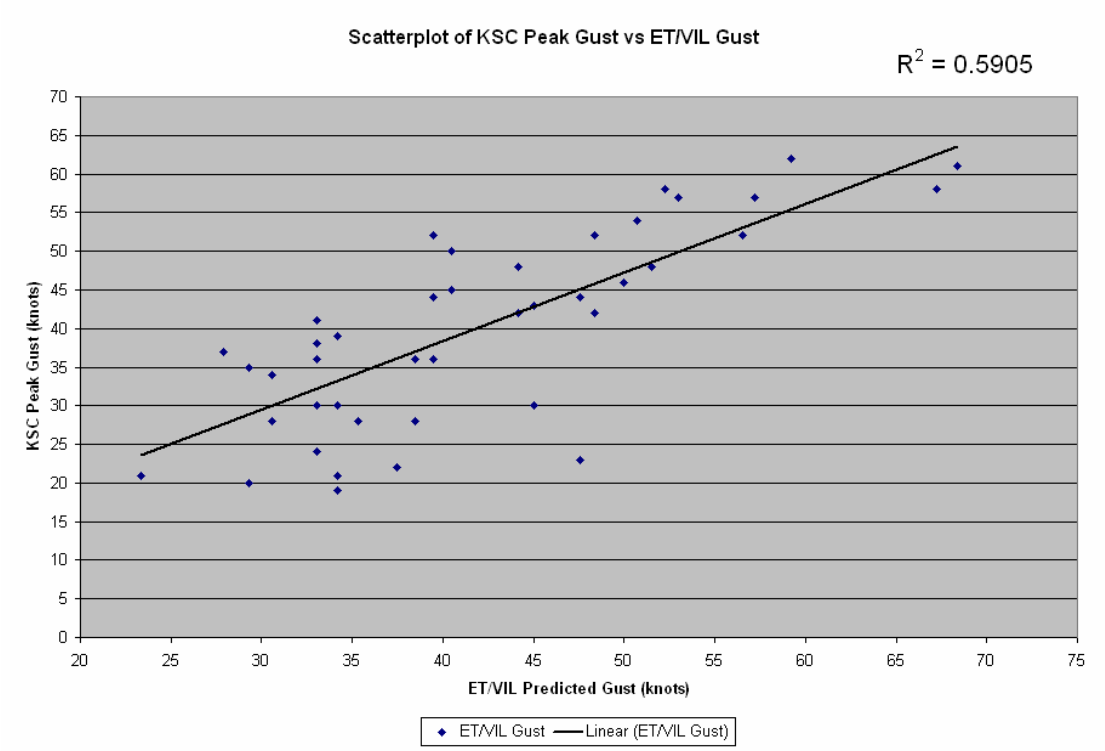

Figure 20. Scatterplot of ET/VIL predicted gust speed vs peak observed gust speed, with correlation coefficient in upper right corner.

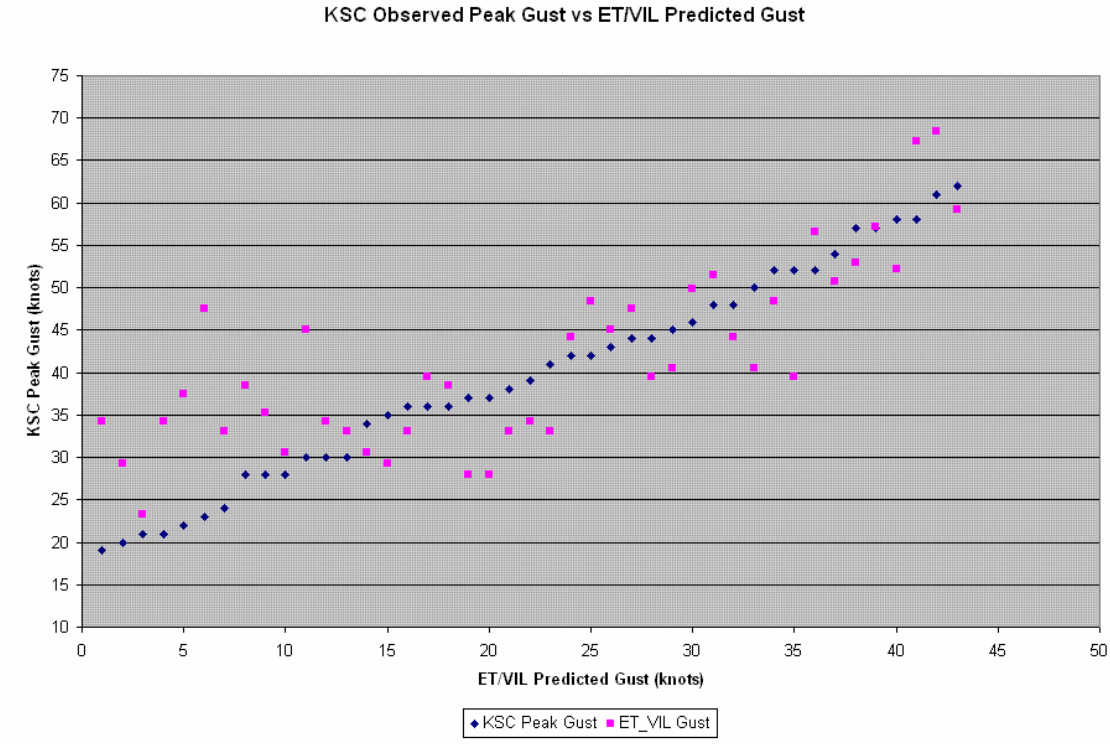

Figure 21. Plot of observed wind gust values versus that predicted by the ET/VIL equation.

. Table 9. Error Statistics Table for ET/VIL.

Category	RMSE	MAE	Hits	% Hits
All Winds	8.1	6.58	26	60.4
Below Criteria	11.5	9.65	5	35.4
Above Criteria	5.93	5.23	21	70.0
35-49 Knots	5.45	4.95	14	68.4
≥ 50 Knots	6.67	5.72	7	54.5

These re-computed errors are found to be much better than those errors reported in Sullivan (1999), who considered only 15 warning criteria wind speeds and found errors that ranged between 9-11 knots and only five “hits.” Looking at the warning-criteria wind speed error calculations in Table 9, those same errors decrease by about 50% and received four times as many “hits” by using a larger dataset.

CHAPTER 5

5. Convective wind forecasting improvements

a. New WSR-88D convective wind gust prediction equation

The Echo Top/VIL Wind Gust Potential Equation was evaluated on the basis of RMS and Mean Absolute errors in the previous chapter. One of the major deficiencies of the ET/VIL relationship that was found from that evaluation was that the ET/VIL equation had undesirably high errors for thunderstorms that produced wind gusts below KSC warning criteria. Thus, because the ET/VIL equation works best for warning-level wind gusts events and not equally as well for < 35 knot wind speeds, it is probably not suited for distinguishing between thunderstorms that produce KSC warning-level wind gust speeds versus those that do not.

To potentially solve this problem (i.e. produce an equation that works reasonably well for all convective wind speeds), a new radar peak wind gust equation has been developed that use some of the Storm Structure cell attributes as predictors using multiple linear regression techniques. This section will present how this equation was developed from a statistical standpoint. Errors will then be calculated using an independent dataset of 22 thunderstorm wind gust events to test its promise as an operational forecast tool.

1) DEVELOPMENT OF REGRESSION EQUATION

Using forward regression predictor selection techniques in Matlab, the following multiple linear regression equation has been developed:

$$GU = (.4138 \times VIL) + (.9194 \times MaxZ) + (.6253 \times height) - 28.7719 \qquad (12)$$

where VIL is the cell-based VIL (in kg m^{-2}), MaxZ is the maximum reflectivity (in dBZ), height is the height of maximum reflectivity (in kilofeet) and GU is the predicted peak wind gust (in knots).

Table 10 displays the ANOVA table for the above regression equation. From the ANOVA table and its components, it appears as though the regression equation is suitable. The F-statistic, a ratio of the mean-squared regression value to the mean-squared residual indicating the relative appropriateness of the model, is arbitrarily high enough to suggest that the regression equation is appropriate. The coefficient of determination, R^2, for this regression equation was found to be .6314, while the adjusted coefficient of determination, R_a^2, was .6031. Both of these values suggest that the predictor variables are reasonably good at explaining any variations in the predictand.

Table 10. ANOVA table.

Source	**Df**	**SS**	**MS**	
Total	43	6410.6		
Regression	3	4047.8	1349.3	F=22.271
Residual	39	2362.8	60.586	

.

In an ideal regression equation, its residuals will be both serially uncorrelated to each other and follow a Gaussian distribution. Figure 22 shows a Normal probability plot (or Q-Q plot) of the regression residuals. A perfect Gaussian distribution is represented by the red dash-dotted line. The closer that

the residuals (given as the blue plus sign marks in Figure 22) follow this line, the better the assumption is that the residuals are to being normally distributed. A perfect Gaussian distribution is represented by the red dash-dotted line. According to the figure, with exception of the upper tail, the residuals do follow an approximately normal distribution. A common test of autocorrelation in the residuals is the Durbin-Watson test. For this regression, the Durbin-Watson test statistic was found to be .8453, with an associated p-value of 5.95×10^{-6}. In this test, the null hypothesis is that the residuals are uncorrelated with an alternative that the residuals are autocorrelated. Based on the p-value, the null hypothesis can be rejected in favor of the alternative hypothesis, resulting in the residuals being autocorrelated. Because the test statistic is small, these residuals are also positively autocorrelated.

2) EVALUATION AND VALIDATION

Figure 23 shows a scatterplot of the KSC observed peak wind gust versus that predicted by Eq. (12) developed above using the independent dataset. Figure 23 shows a strong linear correlation between the observed peak wind gust versus that predicted by Eq. (12).

To assess any biases in Eq. (12), Figure 24 shows a plot of the observed peak wind gust versus that predicted by Eq. (12). The largest errors appear to be for the strong to severe wind speeds (≥ 50 knots), but there does not appear to be any characteristic under- or over-forecasting bias between all wind speeds.

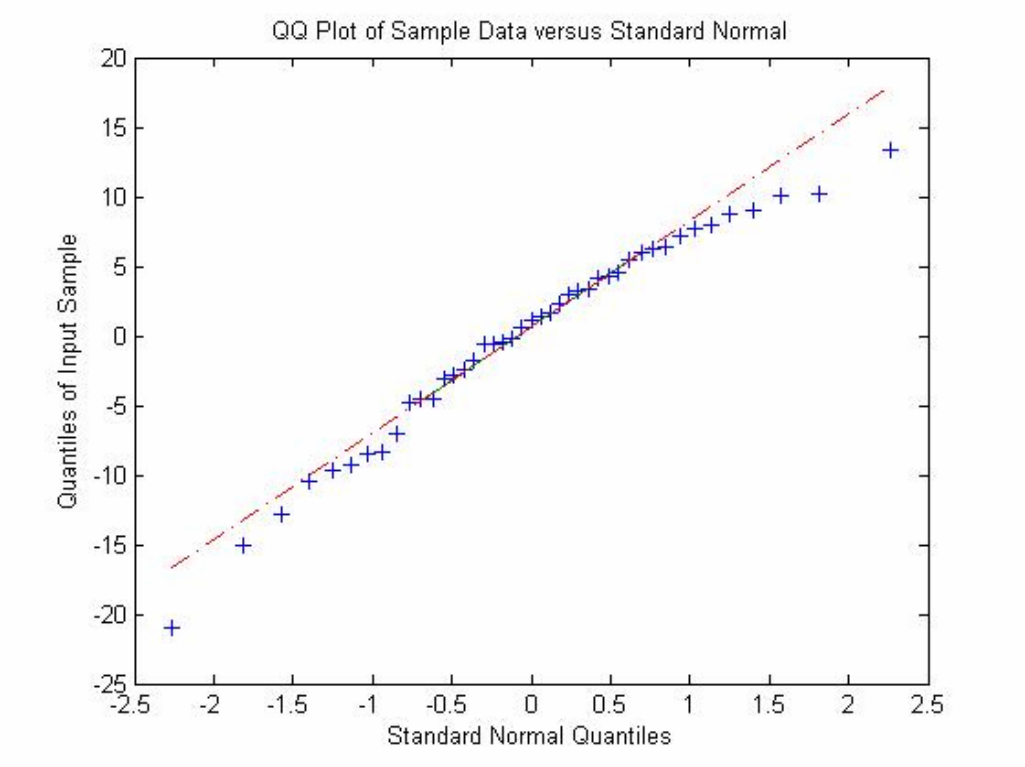

Figure 22. Q-Q plot of regression residuals.

.

Table 11 shows the error statistics table for Eq. (12). Based on the table, there is a much more accurate error for the below-criteria wind speeds compared to that from the ET/VIL equation (compare Table 9 in Chapter 4 to Table 11 that follows). However, errors are slightly higher for above-criteria wind speeds, but most of these errors come from the higher errors reported for ≥ 50 knot wind speeds. Generally speaking, however, compared to the ET/VIL equation for all convective wind speeds, there is about a 1-2 knot improvement in the error using Eq. (12). Much of this improved accuracy is due to the fact that below-criteria wind speeds were predicted with greater than 50% better accuracy.

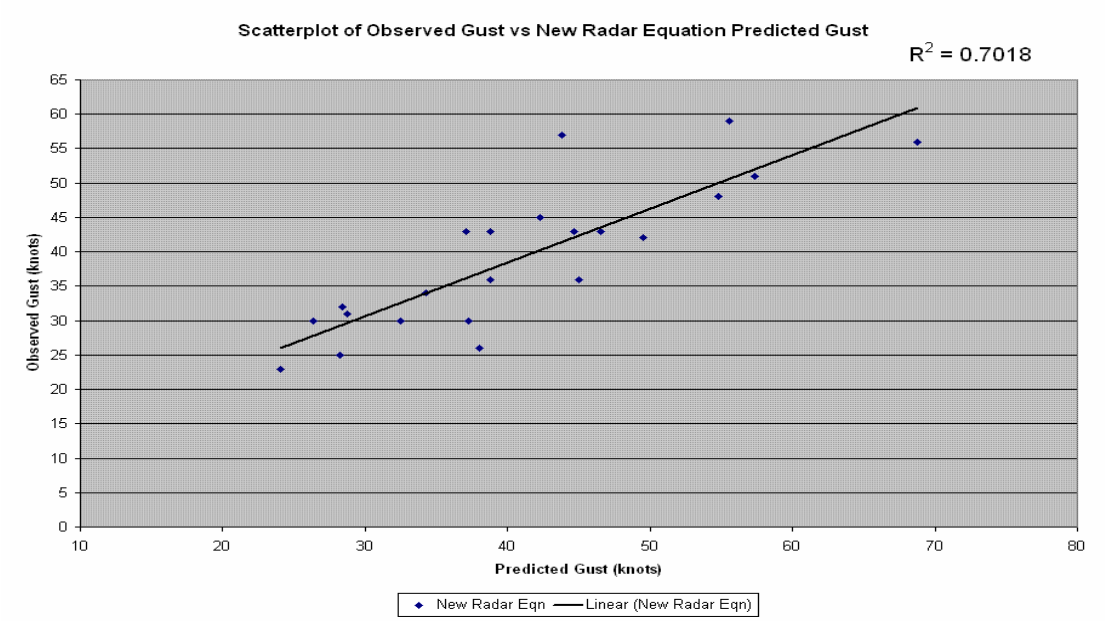

Figure 23. Scatterplot of observed versus predicted peak wind gusts using Eq. (12).

b. Forecasting warning-criteria convective winds using theta-e lapse rates

In Chapter 3, it was found that two RAOB-based convective wind gust forecasting aides—the MDPI and WMSI—both correctly and incorrectly forecast KSC convective wind warning-criteria episodes at approximately equal probabilities (~50%). It was also found that both of these tools appear to forecast convective wind warning episodes under westerly flow regimes (see Chapter 2 and Lericos *et al.* (2000)) with better accuracy, but are not nearly as successful at forecasting the same with the other flow regimes. Because westerly flow convective wind days possess the highest climatological frequency of warning-criteria wind episodes as well as the highest mean convective wind speed (see Figure 6 in Chapter 3), the warning-level wind gusts that occur under the other flow regimes are viewed as being "unanticipated" from a forecasting perspective.

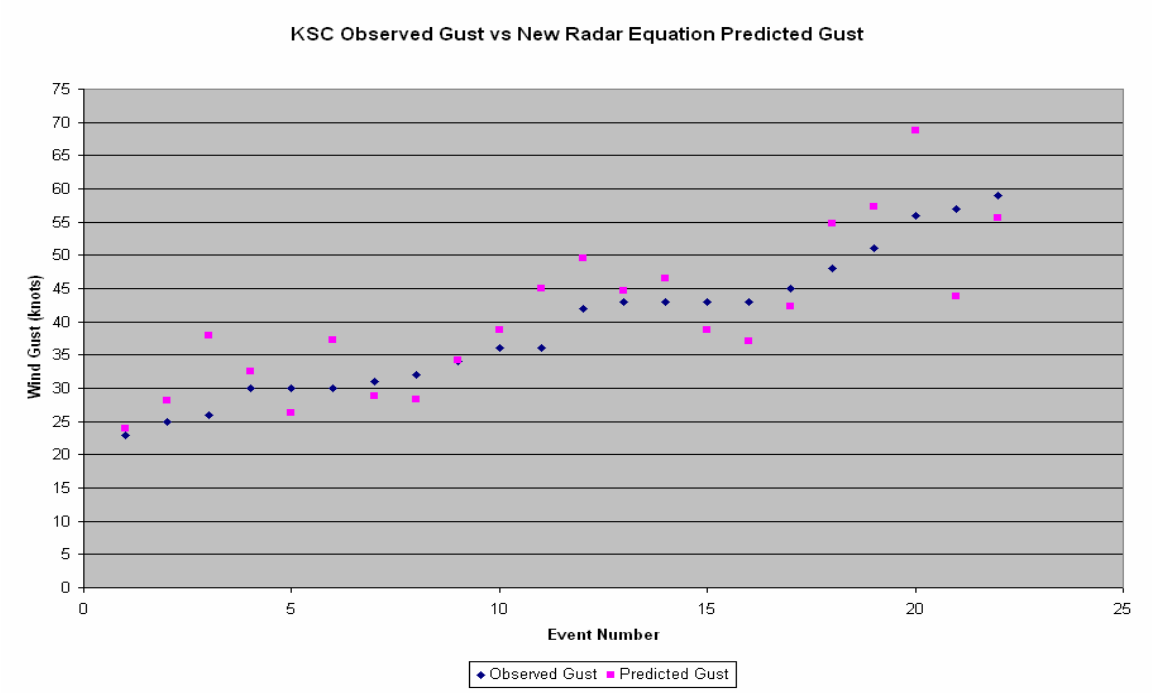

Figure 24. Plot of peak observed gust versus predicted from Eq. (12).

Table 11. Error Statistics Table for Eq. (12).

Category	RMSE	MAE	Hits	%Hits
All Winds	6.39	5.25	13	59.02
Below Criteria	5.22	3.96	7	77.78
Above Criteria	7.09	6.14	6	46.1
35-49 Knot	5.44	4.9	5	55.56
≥ 50 Knot	9.85	8.92	1	25

1) CLIMATOLOGICAL MEAN VERTICAL THETA-E PROFILES

Figure 25(a) shows a comparison of the mean vertical profile of equivalent potential temperature for warning-level convective wind gust days and for below-warning criteria convective wind gust days, while Figure 25(b) shows the associated p-value from comparing the two categorical profiles via a Student's t

test, assuming that there is no significant difference between the profiles as being the null hypothesis. Figure 25(a) shows that in the mean, warning-level convective wind gusts have warmer equivalent potential temperatures at lower levels and slightly cooler equivalent potential temperatures at or slightly above 3 km then those for below-criteria convective wind episodes. Thus, warning-level gusts are more likely to have a strong lapse rate of theta-e. This suggests that examining the theta-e lapse rates could be used as a basis for issuing convective wind gust warnings at the KSC/CCAFS complexes

Figure 25(b) indicates that not all vertical layers of mean theta-e are statistically significant at the 95% level. However, the lower layers (~0-2 km) and a layer just above 3 km are found to be 95% significantly different. These results might suggest that the lapse rate of theta-e be calculated as:

$$LR = \frac{\theta_e - \theta_e^*}{\Delta z} \qquad (13)$$

where LR represents the theta-e lapse rate (in K km^{-1}), θ_e is the maximum theta-e value encountered from the 0-1 km layer (in Kelvin), θ^*_e is the first minimum theta-e encountered at or above 3 km (in Kelvin), and Δz represents the height difference (in kilometers) between the maximum theta-e and minimum theta-e as previously defined.

2) ESTABLISHING THRESHOLD VALUES OF THETA-E LAPSE RATE BY FLOW REGIME USING ROC DIAGRAMS

Figure 26 shows the ROC diagram for the SW-1 flow regime. Based on Figure 26, a value of theta-e lapse rate of 7.0 K km^{-1}, as computed by Eq. (13), yields a POD of .76 and a FAR of .31.

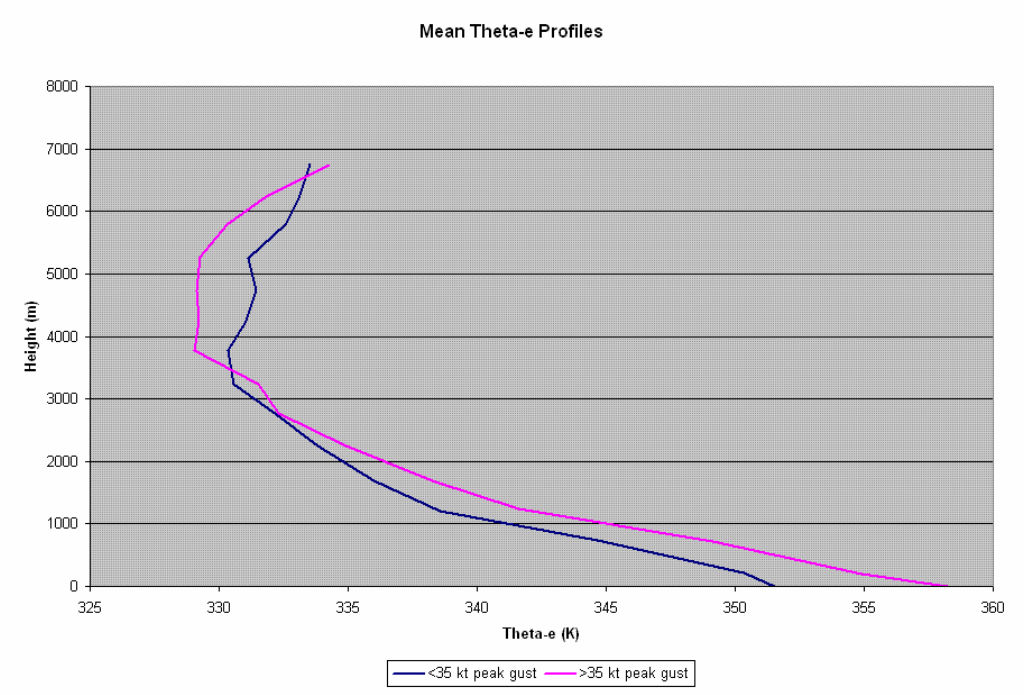

(a)

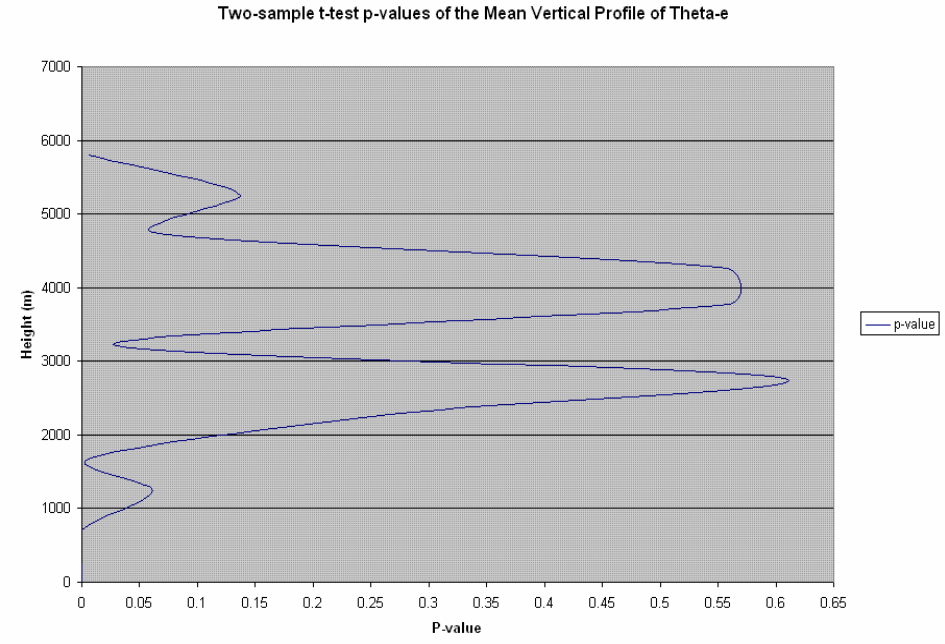

(b)

Figure 25. (a) Mean vertical profiles of theta-e and (b) associated p-values.

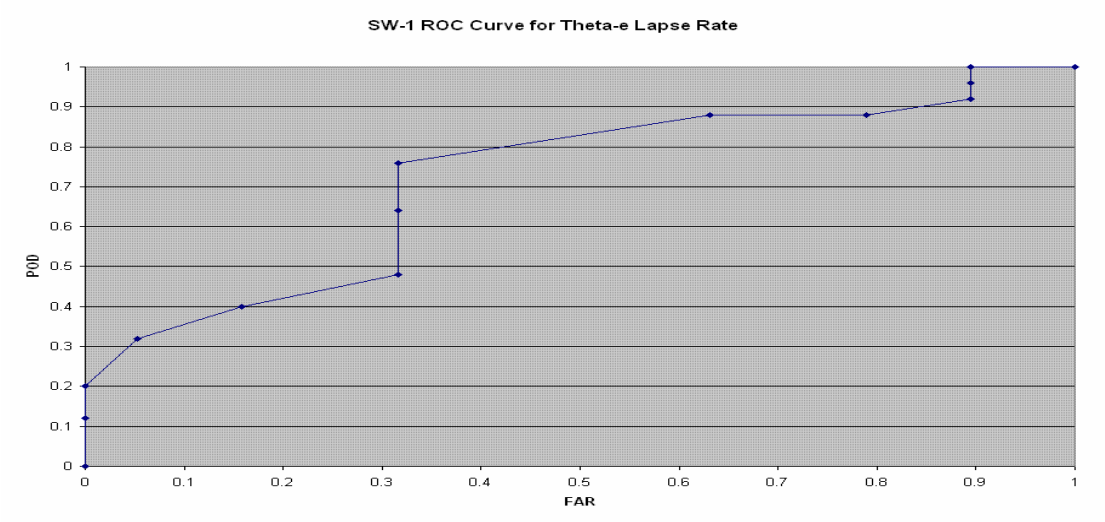

Figure 26. ROC diagram for the SW-1 flow regime.

Figure 27 shows the ROC diagram for the SW-2 flow regime. Note the markedly linear trend that is shown in Figure 27. This implies that as the POD increases, so does the FAR, suggesting a little less reliability. The optimum theta-e lapse rate as computed by Eq. (13) above was found to be 8 K/km^{-1}. Using this threshold value, results in a POD of .59 and a FAR of .41. Note the markedly linear trend that is shown in Figure 27.

Figure 28 shows the ROC diagram for the SE-1 flow regime. Examining Figure 28, a lapse rate value of 9.0 K km^{-1} results in a POD of .55 with a FAR being a low .18.

Figure 29 shows the ROC diagram for the SE-2 flow regime. Here, a theta-e lapse rate value of 5.9 K km^{-1} yields a POD of .75 and a FAR of a low .19. Here, a theta-e lapse rate value of 5.9 K km^{-1} yields a POD of .75 and a FAR of a low .19.

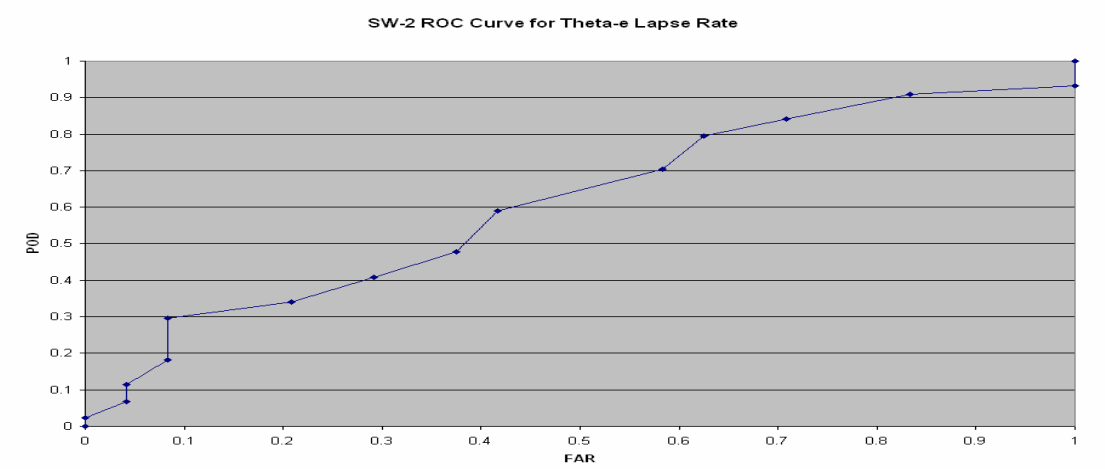

Figure 27. As in Figure 26,for the SW-2 flow regime.

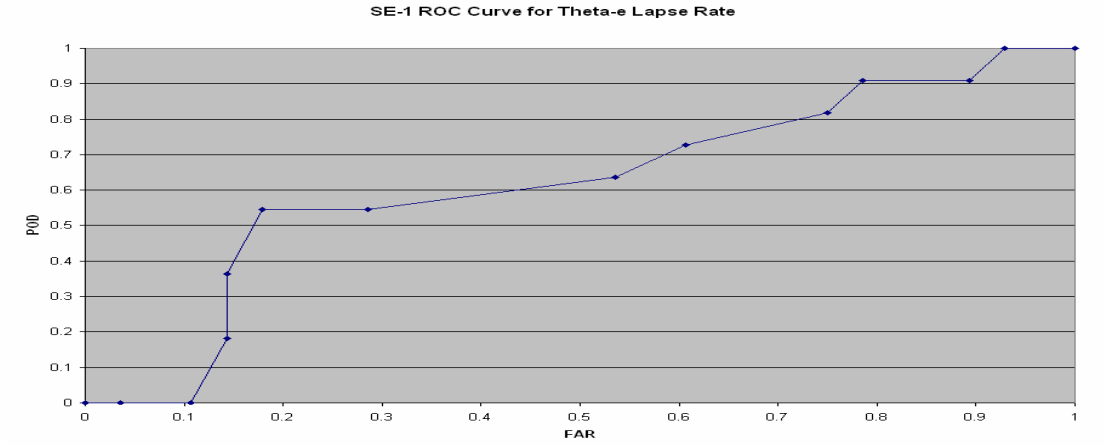

Figure 28. As in Figure 26, but for the SE-1 flow regime.

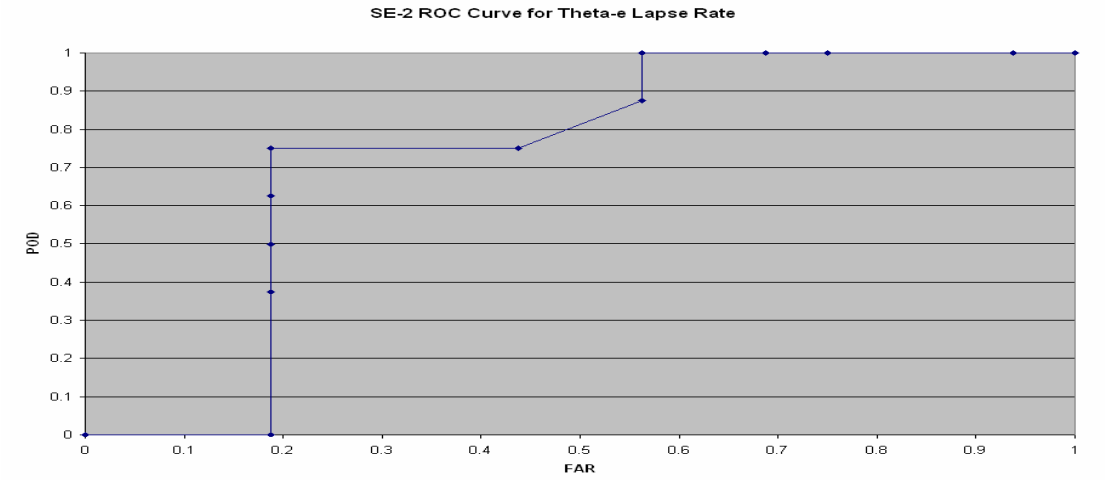

Figure 29. As in Figure 26, but for the SE-2 flow regime.

Figure 30 shows the ROC diagram for the Other flow regime. Figure 30 With that in mind, a theta-e lapse rate value of 8.0 K km^{-1} results in a POD of .51512 and a FAR of .358.

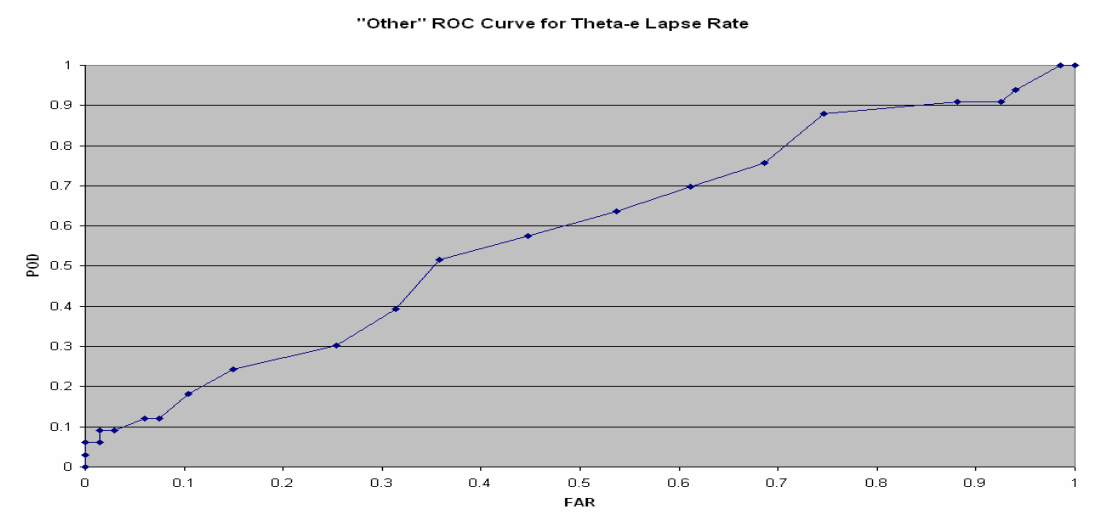

Figure 30. As in Figure 26, but for the Other flow regime.

To summarize these results, the optimum values of theta-e lapse rate that were found from the ROC procedures are presented for all flow regimes in Table 12. Forecasters should recognize that for the PAN, NW, NE and Missing flow regimes, the optimal lapse rates for these may not be accurate because a small number of cases were used for these respective flow regimes. Because of the small number of cases, the ROC diagrams for each of these respective regimes have oddly-shaped curves. Thus their ROC diagrams for these four other flow regimes are not presented here; for completeness however the optimal values of theta-e lapse rate are presented from the diagrams constructed for these small-sampled flow regimes.

Table 12. Summary of optimal theta-e lapse rates using ROC procedures.

Flow Reg.	Theta-e Lapse Rate Value (K km-1)	POD	FAR
SW-1	7	0.76	0.31
SW-2	8	0.59	0.41
SE-1	9	0.55	0.18
SE-2	5.9	0.75	0.19
Other	8	0.52	0.36
Missing	6.5	0.75	0.9
NW	6.5	1	0
NE	5	0.75	0.93
PAN	9.5	0.75	0

CHAPTER 6

6. Discussion and summary

a. Short-term forecasting of convective winds using Doppler radar techniques

There are a couple of caveats and/or considerations that pertain to the radar results presented in Chapter 4 that are worth mentioning here. The first of these is that the computation of the various storm cell attributes from the SCIT algorithm that were analyzed in Chapter 4 are dependent on the scan strategy and volume coverage pattern (VCP) to which the Melbourne, FL Doppler radar is set. Different VCP patterns have different numbers of vertical levels that are sampled. Because parameters such as cell-based vertically integrated liquid and maximum reflectivity, for example, depend in part on the number of vertical levels sampled by the radar, these values would potentially be different for different VCPs and might affect the results presented in Chapter 4. Secondly, all of the radar results only consider storm cell attributes that occur one volume scan prior to the observation of the peak convective wind gust.

1) PREDICTING CONVECTIVE WIND SPEEDS USING THE ET/VIL EQUATION OR EQ. (12)

Some factors to acknowledge when considering the error statistics in Tables 10 and 11 in Chapters 4 and 5 for the ET/VIL equation or Eq. (12) relate to sampling of the downdraft using the KSC tower mesonet in terms of cell location and in terms of certain physical properties of the downdraft. While the KSC mesonet is probably one of the best instrumented locations certainly in the United States to sample wet microburst winds, the two predictive equations

assume that the peak gust would occur directly underneath the cloud base. It would thus require a mesonet tower to be directly underneath the base and receive a direct hit from the downburst core in order for this assumption to be met. In most if not all cases this assumption is not valid. In most scenarios the core of a downburst is located at some distance from a nearby mesonet tower, and so the tower would probably only be sampling the "fringe" wind speeds associated with the vortex ring that surrounds the microburst. Studies by Fujita (1984) and as described in Rinehart (2004) note that the downburst core can tilt essentially as a function of the parent thunderstorm speed. For slow-moving or stationary thunderstorms, the downburst core is more vertical, with wind speeds accelerating out at the same rate isotropically. For thunderstorms that are fast-moving, the core of the downburst would be tilted horizontally downwind of the storm's motion. Since most thunderstorms in east-central Florida during the summertime are typically slow-moving most downburst core orientations are probably more vertical, but some locally faster-moving cells could be observed to occur along sea-breeze/gust-front boundary collisions resulting in more horizontal tilting of the downburst core. Neither of the equations consider terms that adjust for either of these two processes.

2) FORECASTING THE ONSET OF SEVERE CONVECTIVE WINDS USING HAIL INDICATORS

Considering the infrequency of occurrence of severe convective windspeeds (~3% of all convective wind speeds; see Figure 7 in Chapter 3), the finding that most ≥ 50 knot convective windspeeds occur with maximum

reflectivity cores above the freezing level is a potentially significant one and one that requires some additional research before being conclusive. From a preliminary standpoint these results are consistent with prior observational and modeling results as documented in Chapter 1. Both melting and evaporation are both phase changes that promote cooling. These preliminary results might suggest that strong convective windspeeds must have additional latent cooling owing to the melting of hail in addition to the latent cooling from any evaporation of raindrops into layers of dry air.

Hailstones will grow in size in the presence of supercooled water droplets. Supercooled droplets tend to become greater in number above the height of the -5°C isotherm. Although it is not known explicity if the maximum reflectivity cores were found to be above this isotherm, since most of the cores were generally 3,000-5,000 ft higher than the freezing level, it could be inferred that most of the cores were near or above this height.

3) Future research using WSR-88D Doppler radar

Because these results only consider radar-derived storm cell attributes one volume scan prior to microburst occurrence, it would be useful to test these results again over longer lead times. This future research idea would most especially be true for the two radar gust equations, where it would be useful to determine how much lead time these two equations can provide. There might be some difficulty in accomplishing this because of problems pertaining to tracking the same storm cell over time. The SCIT algorithm can “drop” cell IDs and its constituent attributes depending on if the cell in question falls below the

minimum reflectivity criteria to be assigned an alphanumeric ID. It would be seemingly impossible to know unambiguously if one was tracking the same cell if a cell ID was dropped and then re-assigned a different cell ID.

Another area of future research would be to consider evaluating other radar-derived parameters. Because this project only considers reflectivity-based parameters, radial-velocity parameters should be evaluated. In particular, storm-relative radial velocity values should be analyzed because of their ability to detect storm-scale circulations such as microbursts. Several authors have shown that mid-altitude radial velocity convergence leads to strong convective windspeeds, so it would be worthwhile to (a) determine if this radial wind convergence signature is also observed for KSC convective winds and (b) determine how much time in advance does the presence of this feature precede warning-level convective windspeeds.

There are several possible future research areas that deal with the possible correlation to predicting ≥ 45 knot convective winds with the potential for hail. First, using an archive of maximum reflectivity and height of maximum reflectivity at various lead times, it would be worthwhile to investigate if the cores reside above freezing level at different lead times. If these findings were found to be true over increasing values of lead time, another possible tool to consider evaluating would be the Hail Index and the output of the Hail Detection Algorithm (HDA) versus the observed KSC peak convective wind gust. The HDA produces as output the Probability of Hail (POH) and the Probability of Severe Hail (POSH), as well as an estimation of the maximum size diameter hail to be

expected from a storm (MEHS). Higher values of POH are achieved when the height of the 45 dBZ echo reaches higher heights above the freezing level. Higher POSH are found when 50 dBZ echo values are present above the -20°C isotherm. It would be useful to investigate the correlation of these three indices (POH and POSH in particular since both values increase when high reflectivity values are found to reside above either freezing level and /or the -20°C height) to the convective wind speed.

With all that said, a potentially significant improvement to short-term convective wind forecasting using Doppler radar will come in the near future, when the current suite of Doppler radars across the U.S. will be equipped with polarimetric capabilities. One of the benefits of polarized radar as applied to convective wind forecasting is differentiating between rain and the presence of hail. Differential reflectivity (Z_{DR}) has been shown to be particularly good at this—in particular, values of Z_{DR} near zero infer the presence of spherical hydrometeors (e.g. hail). If the presence of hail is required for strong/severe warning-level convective winds, forecasters might look for near-zero Z_{DR} values as being possibly associated with these windspeeds.

b. Forecasting KSC convective winds using radiosonde observations

1) FORECASTING THE LIKELIHOOD OF KSC WARNING-LEVEL CONVECTIVE WINDS USING MDPI AND WMSI

It is apparent from the monthly evaluation of MDPI and WMSI that both indices perform generally better in mid-summer. One reason for the better accuracy in both indices (in particular the MDPI) during the July to August

months may simply be because the boundary layer is warmer, moister and more potentially unstable than during the earlier months of May and June. This would result in making it more favorable to achieve the various convective wind warning thresholds for these two indices. It was also shown in the monthly evaluation of these two indices that the WMSI had much higher false alarm rates than MDPI. This is probably due to the fact that the denominator is probably too small to be a "filtering factor" that Pryor and Ellrod (2004) had intended it to be with regards to KSC convective wind forecasting. CAPEs during the warm-season are above 1000 J kg^{-1} quite commonly and so the current WMSI equation might capture more below-criteria convective wind days. Increasing the denominator might result in a lower false alarm rate for WMSI.

Based on Figures 9 and 10 in Chapter 3, it was shown that both MDPI and WMSI generally forecast westerly flow-regime warning-level winds adequately at best, but have essentially little skill in detecting the same for the other flow regimes. It should first be noted that there was a non-uniform number of events sampled for each flow regime (e.g. a greater number of convective wind days were present for westerly flow regimes than the number for the NE flow regime, for example). For flow regimes where convective winds occur infrequently, it might show more accurate forecast skill scores for those flow regimes where convective winds occur infrequently by increasing the number of convective wind events for those flows. With the sampling considered, it might suggest that there are other factors that might generate warning-level events under these regimes that aren't captured by these two indices.

2) Forecasting the maximum peak convective wind gust using RAOB-based tools

Figure 13 and Table 6 in Chapter 3 suggest that there doesn't appear to be a great deal of promise from any of the four peak convective wind gust forecasting aides that use RAOB data as input. Based on Figure 13, both the previously unevaluated Snyder Method and the T1 gust forecasting tools show large systematic errors indicating that these two indices are not detecting the proper generating mechanisms for KSC convective winds. The only remaining maximum peak convective wind speed forecasting tools are the T2 and WINDEX which only adequately at best predict the maximum peak convective windspeed.

The Snyder method has a low bias for all convective wind speeds. The Snyder method includes a mean windspeed term in its computation that uses the mean wind from 5000 ft above and below the wet-bulb zero height as input. It is hypothesized that much of the low bias is from this term because windspeeds aloft in the Florida warm-season are weak. Thus the Snyder Method is probably best suited for areas other than Florida for detecting microburst winds. The T1, on the other hand, has a systematic high bias which results in—misleadingly--fairly accurate predictions of strong to severe convective windspeeds, but gross overestimates of the peak convective windspeed for peak convective windspeeds between 35-45 knots. While the T1 also includes a mean windspeed factor, because the mean wind speed is climatologically small, removing the mean wind speed from the T1 gust speed calculating would likely still result in large errors.

From Figure 13, the WINDEX has predictive values that are highly variable. Although these dramatic drops or rises were not closely investigated, Ellrod *et al.* (2000) found that WINDEX is probably an underestimator of convective winds at night owing to the more stable lapse rate at night. In the WINDEX computation, if the square of the surface-to-melting level lapse rate is less than 35, this term is set to zero. This condition is more likely to be met at night when the sun is not out to warm the ground. This might explain a number of the very low predictions for the windspeed.

3) PREDICTING THE LIKELIHOOD OF WARNING-LEVEL CONVECTIVE WINDS BY USING THRESHOLD THETA-E LAPSE RATES

It was shown in Figure 25, Table 11 and in the ROC curves in Chapter 5 that there appears to be promise in using threshold values of lapse rate of theta-e with the thresholds defined by flow regime. Using any given flow regime, a forecaster would be allowed to assess the threat of lightning and then assess the risk of warning-level convective windspeeds should lightning be a significant risk.

There doesn't appear to be any favored flow regime bias using the theta-e lapse rate thresholds. This can't be said for the MDPI or WMSI, in which both show better accuracy for westerly flow regimes only. As in the MDPI and WMSI evaluations one must consider that there were a larger number of convective winds on westerly flow regime days than on much less frequently occurring flow regimes. For these flow regimes, this leads to a ROC curve that isn't curvilinear but is more irregularly shaped owing to the small number of data points. Results for these flow regimes are not as conclusive because of limited sampling.

4). FUTURE RESEARCH USING RAOB-BASED FORECASTING TOOLS

As a first possible area of future research, some descriptive statistics of relevant RAOB parameters (e.g. CAPE, LI, PW, etc…) to convective wind gust forecasting should be calculated for (a) below-criteria and above-criteria convective wind days and (b) for all convective wind speeds. Loconto and Koermer (2005) presented some summary statistics for several convective wind forecasting parameters from XMR RAOB data but use a small 10-case dataset. Any possible differentiating trends between below-criteria convective wind RAOB parameters versus those for above-criteria convective winds should be tested for statistical significance.

One area that should receive consideration for possible future research in using KXMR RAOB data for prediction of KSC convective winds is in the development of a new maximum peak wind gust forecasting tool and have it be tested against an independent dataset so that errors could be computed. None of the 4 predictive equations were found to show much operational promise, which underscores the need for a new predictive gust tool that uses RAOB-derived parameters.

Another area of potential future research is in the development of monthly mean vertical plots of theta-e (e.g. similar to that of Figure 25). Figure 25 considers an entire warm-season average of the theta-e for above-criteria winds versus below-criteria winds. Because the mean vertical profile of theta-e in May might be quite different than the overall warm-season mean profile (from possibly colder low-level theta-e values and colder upper-level theta-e values), it might be

interesting to compose monthly mean vertical profiles of theta-e to see how these profiles vary by month.

c. Thesis summary

The primary goal of this Master's Thesis was to develop two things that pertain to warm-season convective wind gust forecasting at NASA's Kennedy Space Center and Cape Canaveral Air Force Station: (a) an evaluation of existing RAOB and WSR-88D Doppler radar forecasting tools and (b) to improve upon such forecasts by developing additional forecasting aids that utilize RAOB and radar data. Using quality-controlled, 5-minute averaged KSC tower mesonetwork peak wind data from over 40 towers between May through September of 1995-2005, in conjunction with radar, satellite, lightning, KTTS METARs and surface maps, periods in which convective wind speeds had occurred were identified. From this chronological pool of "convective wind periods", a sample of dates were selected in which KXMR RAOB data and/or Storm Structure WSR-88D storm cell attributes were analyzed. Particular emphasis was placed on distinguishing between days in which maximum convective peak wind speeds of ≥ 35 knots was measured (considered to be "KSC warning-criteria") versus those that were < 35 knots.

Using a suite of forecast skill/error metrics on RAOB-based forecasting tools, several strengths/weaknesses were unearthed. The Microburst Day Potential Index (MDPI) and Wet Microburst Severity Index (WMSI), both of which are yes/no predictors of warning-criteria convective wind speeds, were found to predict a positive detection and a false alarm of warning-level convective winds

at essentially the same probability (~50%). Monthly assessments of MDPI and WMSI forecasts suggest that both indices have better accuracy as the warm-season gets longer, with a peak in accuracy in the month of August. From a listing of Florida flow regimes defined by the location of a surface ridge axis that extends across the Florida peninsula emanating from the Bermuda High (Lericos *et al.*, 2000) it is shown that both MDPI and WMSI best forecast warning-criteria winds on days when the flow is westerly. While westerly flows correspond to climatologically-favored flow regimes for thunderstorms and convective winds across the Space Coast, these two indices do not forecast easterly and northerly flows very well. These indices are also not good at detecting warning-criteria winds when the surface ridge is directly over the area. In addition to these results, an error evaluation of 4 prominent RAOB-based maximum peak convective wind speed forecasting tools showed that none of these tools were consistently successful at predicting the observed peak convective wind speed. Of these 4, the T2 Max Predicted Gust was shown to be the most accurate, with RMS errors on the order of ~9 knots. Two of these tools, the T1 and Snyder method, appeared to have systematic errors that resulted in large RMS errors. These errors are likely due to the fact that there are terms in the T1 and Snyder Method's computations that are (a) small and/or (b) quantify physical processes that are not likely to be involved in generating warm-season convective winds at KSC/CCAFS. The numerous flaws that were discovered in these RAOB-derived tools further underscored the need for convective wind forecasting improvements.

Scatterplots of several Doppler radar-derived storm cell attributes (cell-based VIL, maximum reflectivity, height of maximum reflectivity, echo tops, and VIL Density) versus the peak observed convective wind speed showed moderately strong correlations between cell-based VIL and maximum reflectivity to the peak convective wind speed. Various error statistics were computed for the Echo Top/VIL (ET/VIL) wind gust potential equation using 43 days in which convective wind speeds occurred. While calculated errors were found to suggest a reasonable accuracy for warning-criteria winds, large overforecasting errors were discovered for below warning-criteria winds. This suggests that the ET/VIL equation is poorly suited for differentiating between warning-level winds versus wind speeds lower than KSC warning-criteria.

Using the maximum reflectivity and height of maximum reflectivity data from the WSR-88D Storm Structure product and the recorded height of the freezing level from the KXMR RAOB, a possible relationship between the prediction of strong to severe convective wind speeds ≥ 45 knots and hail indicators was discovered. More specifically, it was observed that strong to severe convective windspeeds had their maximum reflectivity cores were found to penetrate above the 0°C level and were coincident with very high values of maximum reflectivity. This result implies the presence of hail. Conceptually, this result suggests that for strong convective windspeeds that the latent cooling associated with the melting of hail be present in addition to any latent cooling owing to the evaporation of raindrops into sufficiently dry enough layers. This preliminary result is consistent with observational (Atlas *et al.*, 2004) and

modeling studies (Srivastava 1985,1987; Proctor 1989) of strong wet microbursts in stable temperature lapse rate environments.

There were two convective wind forecasting improvements/aids that were developed in this thesis—a new predictive maximum convective peak wind gust tool and threshold values of theta-e lapse rate defined by the flow regimes in Lericos et. al. (2000). The new predictive radar gust equation was developed using multiple linear regression techniques. This equation includes cell-based VIL, maximum reflectivity and height of maximum reflectivity as predictors. The same errors as were computed for the ET/VIL equation were computed for the new equation using a separate 22 case dataset. Not only were the errors for all convective windspeeds for this new equation found to be 1-2 knots more accurate, but below-criteria windspeeds had very low errors, with errors only about 1-2 knots less accurate for warning-level events as compared to ET/VIL. Because of the much greater success at predicting below-criteria winds, this equation is viewed as an improvement that has the potential to show much operational promise. Based on a plot of mean vertical profiles of theta-e, it was found that one possible distinguishing factor between warning-criteria winds to below-criteria winds may be a steeper theta-e lapse rate that uses the first minimum theta-e value encountered at or above 3 km. Using a statistical procedure called Relative Operating Characteristics (ROC), threshold values of theta-e lapse rate were established for each flow regime. Using the optimal values of theta-e lapse rate for each flow regime results in better accuracy at

predicting warning-level convective windspeeds regardless of westerly or easterly flow regime.

REFERENCES

Atkins, N.T., and R.M. Wakimoto, 1991. Wet microburst activity over the southeastern United States: Implications for forecasting. *Weather and Forecasting*, **6,** 470-482.

Atlas, D., C.W. Ulbrich, and C.R. Williams, 2004. Physical origin of a wet microburst: Observations and theory. *Journal of the Atmospheric Sciences,* **61,** 1186-1196.

Blanchard, D.O., 1998. Assessing the vertical distribution of convective available potential energy. *Weather and Forecasting,* **13,**870-877.

Case, J.L. and W.H. Bauman III, 2004. A Meso-Climatology Study of the High-Resolution Tower Network Over The Florida Spaceport. *11th Conf. on Aviation, Range, and Aerospace Meteorology*, 4-8 October 2004, P7.6.

Cummings, K.A., E.J. Dupont, A.N. Loconto, J.P. Koermer and W.P. Roeder, 2007. An updated warm-season convective wind climatology for the Florida Space Coast. Preprint CD-ROM, *16th Conf. of Applied Climatology, Jan 2007.*

Ellrod, G.P., J.P. Nelson, M.R. Witiw, L. Bottos, and W.P. Roeder, 2000. Experimental GOES sounder products for the assessment of downburst potential. *Weather and Forecasting*, **15,** 527-541.

Emanuel, K.A., 1981. A similarity theory for unsaturated downdrafts within clouds. *Journal of the Atmospheric Sciences,* **38,** 1541-1557.

Falk, K., L. Harrison, and J. Elmore, 1998. Preliminary downburst climatology and warning guidelines from a single-cell thunderstorm database. NOAA Technical Memorandum NWS SR/SSD 98-31, National Weather Service, Southern Region, Fort Worth, TX. [Available online at http://www.srh.noaa.gov/shv/Downburst_Climo.html]

Fujita, T.T., 1981. Tornadoes and downbursts in the context of generalized planetary scales. *Journal of the Atmospheric Sciences,* **38,** 1511-1534.

Geerts, B., 2001. Estimating downburst-related maximum surface wind speeds by means of proximity soundings in New South Wales, Australia. *Weather and Forecasting,* **16,** 261-269.

Koermer, J.P., and A.N. Loconto, 2005. CCAFS / KSC Convective Wind Study Interim Report. NASA Contractor Report NGT5-40088 (Subcontract 01-530). 36 pp.

Lambert, W.C., 2002. Statistical short-range guidance for peak wind speed forecasts on Kennedy Space Center/Cape Canaveral Air Force Station: Phase I results. NASA Contractor Report CR-2002-211180. 39 pp.

Lericos, T.P., H.E. Fuelburg, A.I. Watson, and R.I. Holle, 2000. Warm season lightning distributions over the Florida Peninsula as related to synoptic patterns. *Weather and Forecasting*, **17,** 83-98.

McCann, D.W., 1994. WINDEX—A new index for forecasting microburst potential. *Weather and Forecasting,* **9,** 532-541.

Miller, R.C., 1975. Notes on analysis and severe-storm forecasting procedures of the Air Force Global Weather Central. Technical Report 200 – Revised. Air Weather Service (MAC), United States Air Force. Chapter 10, pp. 10.1-10.5.

Miller, S.T.K., 2006. Skew-t tutorial. Viewed March 18, 2006. [Available online at http://vortex.plymouth.edu/~stmiller.html]

Proctor, F.H., 1989. Numerical simulations of an isolated microburst. Part II: Sensitivity experiments. *Journal of the Atmospheric Sciences,* **46,** 2143-2164.

Pryor, K.L. and G.P. Ellrod, 2004. WMSI: A new index for forecasting wet microburst severity. *National Weather Association Electronic Journal of Operational Meteorology,* 2004-EJ3. [Available online at http://www.nwas.org/ej/pdf/2004-EJ3.pdf]

_____, and G.P. Ellrod, 2004. Recent improvements to the GOES microburst products. *Weather and Forecasting,* **19,** 582-594.

Roberts, R.D., and J.W. Wilson, 1989. A proposed microburst nowcasting procedure using single-Doppler radar. *Journal of Applied Meteorology,* **28,** 285-303.

Sanger, N., 1999. CCAS microburst climatology. M.S. thesis, Dept. of Meteorology, Texas A&M University, College Station, TX. [Available from College of Geoscience, Texas A&M University, College Station, TX 77843-3148.]

Srivastava, R.C., 1985. A simple model of evaporatively-driven downdraft: Application to microburst downdraft. *Journal of the Atmospheric Sciences,* **42,** 1004-1023.

_____, 1987. A model of intense downdrafts driven by the melting and evaporation of precipitation. *Journal of the Atmospheric Sciences,* **44,** 1752-1773.

Stewart, S.R., 1996. Wet microbursts—Predicting peak wind gusts associated with summertime pulse-type thunderstorms. Preprints, *15th Conf. on Weather and Forecasting.* Amer. Meteor. Soc., 324-327.

Sullivan, G.D., 1999. Using WSR-88D to Forecast Convective Winds at the Kennedy Space Center and Cape Canaveral Air Station. M.S. thesis, Air Force Institute of Technology. 97 pp.

Wheeler, M., 1996. Verification and Implementation of Microburst Day Potential Index (MDPI) and Wind Index (WINDEX) forecasting tools at Cape Canaveral Air Force Station. NASA Contractor Report CR-201354, 24 pp.

_____, and W.P. Roeder, 1996. Forecasting wet microbursts on the central Florida Atlantic Coast in support of the United States Space Program. Preprints, *18th Conf. on Severe Local Storms*. Amer. Met. Soc., 654-658.

Wilks, D.S., 2006. Statistical Methods in the Atmospheric Sciences. 2nd ed. Academic Press, 627 pp.

Wilson, J.W., R.D. Roberts, C. Kessinger, and J. McCarthy, 1984. Microburst wind structure and evaluation of Doppler radar for airport wind shear detection. *Journal of Applied Meteorology,* **23**, 898-915.